



## Cod liver oil nano-structured lipid carriers (Cod-NLCs) as a promising platform for nose to brain delivery: Preparation, *in vitro* optimization, *ex vivo* cytotoxicity & *in vivo* biodistribution utilizing radioiodinated zopiclone

Esraa Taha<sup>a</sup>, Samia A. Nour<sup>a</sup>, Wael Mamdouh<sup>b</sup>, Adli A. Selim<sup>c</sup>, Mohamed M. Swidan<sup>c</sup>, Ahmed B. Ibrahim<sup>c</sup>, Marianne J. Naguib<sup>a,\*</sup>

<sup>a</sup> Department of Pharmaceutics and Industrial pharmacy, Faculty of Pharmacy, Cairo University, Cairo, Egypt

<sup>b</sup> Department of Chemistry, School of Sciences and Engineering, The American University in Cairo (AUC), AUC Avenue, P.O. Box 74, New Cairo 11835, Egypt

<sup>c</sup> Labeled Compounds Department, Hot Labs Center, Egyptian Atomic Energy Authority, PO13759, Cairo, Egypt.

### ARTICLE INFO

#### Keywords:

Radioiodinated zopiclone  
Nano lipid carriers  
Brain targeting  
Insomnia  
Cod liver oil  
Intranasal drug delivery

### ABSTRACT

Nano-structured lipid carriers containing zopiclone were prepared as a targeted drug delivery system to convey zopiclone directly to brain *via* nasal route. Nano-structured lipid carriers were constructed adopting hot emulsification-ultrasonication method using palmitic acid in place of the solid lipid, cod liver oil as liquid lipid, and poloxamer 407 as a surfactant. A three-factor three-level central composite face-centered design was used to optimize the formulated nano-structured lipid carriers. The independent factors were lipid amount ( $X_1$ ), surfactant amount ( $X_2$ ), and sonication time ( $X_3$ ). The examined responses were entrapment efficiency ( $EE, Y_1, \%$ ), particle size ( $PS, Y_2, nm$ ), zeta potential ( $mV$ ), polydispersity index ( $PDI, Y_3$ ), *in vitro* release ( $Q_{8h}, Y_4, \%$ ) and dissolution efficiency ( $DE, Y_5, \%$ ). The optimum formula showed high entrapment efficiency of  $94.31\% \pm 2.44$ , *in vitro* drug release of  $83.89\% \pm 1.77$  with dissolution efficiency equals  $88.63\% \pm 2.01$ , small particle size of  $71.27 nm \pm 13.57$  and low polydispersity index  $0.097 \pm 0.15$ . *In vivo* biodistribution in mice was evaluated by a radiobiological technique using radioiodinated zopiclone ( $[^{131}I]$ iodo-ZP). Results revealed the superiority of the intranasal route to deliver zopiclone directly to brain faster and higher brain uptake ( $6.9 \pm 1.02\%ID/g$  at 5 min post-administration). The current study confirmed that intranasal administration of nano-structured lipid carriers had great potential as an effective tool for targeted brain zopiclone delivery for insomnia treatment.

### 1. Introduction

Insomnia is the most common sleep disorder among the population with prevalence estimates extending from 5 to 50% (Mattos et al., 2021). It is described as difficulty in initiating or continuing sleep as well as poor sleep quality for at least three months (Weitzer et al., 2021). Chronic insomnia requires medical intervention as there is a strong correlation between insomnia, anxiety, and depression. Insomnia is even a symptom of almost all mental health disorders (Van Someren, 2021). Not only this, insomnia has been proven to be linked with the incidence of cardiovascular diseases morbidity, and mortality (Javaheri and Redline, 2017). Treatment mainly involves the use of hypnotics. Benzodiazepines were widely used for decades as very effective hypnotics since they were introduced, but their side effects of tolerance and physical dependence create the need for safer drug candidates. This led

to the development of non-benzodiazepines or as known 'Z-drugs' (Bragg et al., 2019); that were introduced to the market in the 1990s (Brandt and Leong, 2017). Z-drugs have fewer side effects owing to their short half-life, selective drug profiles, and fewer drug-drug interactions (Zaami et al., 2021). Zopiclone (ZP) is a type A  $\gamma$ -aminobutyric acid (GABA) receptor agonist that increases GABA-neuronal block (Louzada et al., 2021b). Zopiclone can overcome the residual side effects caused by benzodiazepines such as difficulty in waking up, low morning concentration, and impaired psychomotor performance (Agravat, 2018; de Mendonça et al., 2021; Koch-Weser et al., 1983), that is why it is considered as a very effective sleep aid, safe and well-tolerated in all age categories (Louzada et al., 2021a; Najib, 2010).

Oral administration of ZP results in a peripheral release of the drug into non-targeted sites, leading to systemic side effects including dry mouth and bitter metallic aftertaste (Louzada et al., 2021a).

\* Corresponding author.

E-mail address: [marian.naguib@pharma.cu.edu.eg](mailto:marian.naguib@pharma.cu.edu.eg) (M.J. Naguib).

<https://doi.org/10.1016/j.ijpx.2023.100160>

Received 20 November 2022; Received in revised form 18 December 2022; Accepted 3 January 2023

Available online 4 January 2023

2590-1567/© 2023 The Authors. Published by Elsevier B.V. This is an open access article under the CC BY-NC-ND license (<http://creativecommons.org/licenses/by-nc-nd/4.0/>).

Furthermore, cytochrome P450 enzyme extensively metabolizes ZP in the liver into two main metabolites, *N*-desmethyl-zopiclone and *N*-oxide-zopiclone. Thirty percent of the dose is *N*-desmethyl-zopiclone, which is pharmacologically inactive (Chouinard et al., 1999; Hesse et al., 2003). This extensive metabolism ultimately leads to dose reduction in individuals over the age of 65, as well as those with renal or hepatic impairment (Goa and Heel, 1986; Noble et al., 1998). Thus nasal administration of ZP can achieve direct nose-to-brain transmission of the drug precluding many limitations bypassing its hepatic metabolism, decreasing side effects in addition to the capability of lowering the dose with rapid onset of action.

Over the past decades, targeted drug delivery systems (TDDS) had always been an attractive area for research for better drug efficiency, lesser side effects, and protection from metabolic or degradation pathways. These metabolic pathways decrease drugs bioavailability at the target site leading to lower therapeutic efficacy and more undesirable effects (Zhang et al., 2019). Away from different body organs, the brain is considered the most protected and shielded one by the entity of blood brain barrier (BBB). The BBB has numerous physical and chemical mechanisms to prevent different molecules either harmful toxins, pathogens, or even beneficial ones from reaching the brain (Agrahari et al., 2019; Sharma et al., 2019). Thus almost all large drug molecules cannot reach the brain after conventional oral or intravenous administration (Crowe et al., 2018). Only molecules with a molecular weight below 400–600 Da can cross BBB (Sahu et al., 2021). Herein, nanoparticles elucidate to offer an ideal solution for the poor permeability of BBB having a very small size scale, being biocompatible and safe make it easily diffuse through BBB through the tight junctions between the endothelial cells facilitating therapeutic agents delivery to the brain (Moura et al., 2019; Tan et al., 2020; Teleanu et al., 2018). Other mechanisms involved in brain uptake include endocytosis and transcytosis which facilitate drug passage through the endothelial cell layer (Saeedi et al., 2019).

The intranasal route proved to be an easy, convenient, and reliable route over conventional routes of drug delivery (oral, intravenous, ... etc.). Intranasal route can effectively achieve direct brain drug delivery through different pathways mainly the olfactory nerve and trigeminal nerve pathways bypassing the BBB, first-pass metabolism and decreasing many off-target side-effects (Keller et al., 2022; Lombardo et al., 2021).

NLCs (nano-structured lipid carriers) are thought to be the next generation of solid-lipid nanoparticles (SLNs). The main difference between NLCs & SLNs is that NLCs are formed by mingling solid and liquid lipids (compared to solid lipids only in SLNs) with certain ratios along with the aqueous phase and surfactants (Mura et al., 2021). This results in lower perfection of the matrix and forming an amorphous structure. Thus allows more drug loading and better encapsulation of either hydrophilic or hydrophobic drugs and less drug leaking from the matrix (Hassan et al., 2022; Shirazi et al., 2021). On the other hand, SLNs yield a perfect crystalline lattice providing very small space for the encapsulation of drug molecules (Katopodi and Detsi, 2021). NLCs are also biocompatible and biodegradable with low *in vivo* toxicity. They are cost-effective with higher storage stability, prolonged drug release, and drug targeting (Tsai et al., 2012).

Generally, one of these radiobiological techniques could be used to properly evaluate *in vivo* biodistribution: a) Drug radiolabeling (Nour et al., 2016) b) Radiolabeling of the optimized formulation (Sayed et al., 2021) c) Using a radiolabeling indicator (Abd El-Halim et al., 2020).

Thus the objective of the existing study was to prepare ZP-loaded NLCs utilizing hot emulsification-ultrasonication method. The prepared ZP-loaded NLCs were composed of palmitic acid (PA) as a solid lipid, cod liver oil as a liquid lipid, and poloxamer 407 (PLX 407) as a surfactant. The goal was to directly deliver ZP to the brain via the nasal route, to minimize its systemic exposure and achieve direct nose to brain transfer. Optimization of ZP-loaded NLCs was done in relation to minimized particle size, maximized entrapment efficiency, and *in vitro*

release. The optimized formula was then evaluated for morphological characters and *ex vivo* cytotoxicity. *In vivo* biodistribution and performance of the optimized zopiclone-loaded NLCs were assessed *in vivo* using radioiodinated zopiclone ( $[^{131}\text{I}]$ iodo-ZP) that was used in radio formulation of  $[^{131}\text{I}]$ iodo-zopiclone-loaded nano lipid carriers ( $[^{131}\text{I}]$ iodo-ZP-NLCs).

## 2. Material and Methods

### 2.1. Materials

Zopiclone was a kind treat from Eva pharm pharmaceutical company, Egypt. Palmitic acid, stearic acid, glyceryl monostearate, Compritol® 888, Poloxamer 407 (PLX 407), Tween 80, polyoxyl 40, methanol, acetone and dialysis membrane (12,000–14,000 Mwt cut off) were all procured from Sigma Aldrich St. Louis, Missouri, USA. Cod liver oil was purchased from Chemajet, Egypt.  $^{131}\text{I}$ iodine was obtained from radioisotope production facility (RPF), Egypt. The remainder of the reagents and chemicals were of analytical grade.

### 2.2. Methodology

#### 2.2.1. Selection of solid lipid

The choice of the solid lipid was made according to the maximum drug solubility (Kovačević et al., 2020). Four lipids were evaluated (stearic acid, palmitic acid, glyceryl monostearate, and Compritol® 888). For screening, 0.5 g of the lipid was melted at 80 °C, and then, in 1 mL of acetone, 10 mg of ZP was dissolved and added to the lipid. The vials were kept on a hot plate magnetic stirrer at 80 °C for 1 h, then the amount of ZP was determined spectrophotometrically (UV-1601 PC; Shimadzu, Kyoto, Japan) at  $\lambda_{\text{max}} = 304 \text{ nm}$  (Zhou et al., 2020) after 10-folds dilution with methanol. The lipid with the maximum drug solubility was chosen for further preparation of NLCs.

#### 2.2.2. Selection of surfactant

Three surfactants were screened (Tween 80, PLX 407, and polyoxyl 40). These surfactants were used at the same concentration (6% w/v) to prepare NLCs. The entrapment efficiency and particle size were measured. The surfactant with higher drug entrapment and smaller particle size was chosen for NLCs formulation (Shinde et al., 2022).

#### 2.2.3. Formulation and optimization of ZP-loaded NLCs

A tailored three-factor three-level ( $3^3$ ) central composite face-centered (CCFD) design-based upon preliminary studies- was employed utilizing Design-Expert®7 (Stat-Ease, Inc., Minneapolis, Minnesota, USA) to explore the effects of three independent variables which were; lipid amount ( $X_1$ ), surfactant amount ( $X_2$ ), and sonication time ( $X_3$ ) at three levels designated as (-1, 0, +1) as shown in Table 1, along with their actual values. The measured responses were entrapment efficiency (EE,  $Y_1$ , %), particle size (PS,  $Y_2$ , nm), polydispersity index (PDI,  $Y_3$ ), zeta potential, *in vitro* release after 8 h (Q8h,  $Y_4$ , %) and

**Table 1**

Variables in  $3^3$  central composite face-centered design (CCFD) for preparation of ZP-loaded NLCs.

| Independent variables                    | Levels                          |     |     |
|--|---------------------------------|-----|-----|
|  | -1                              | 0   | 1   |
| $X_1$ : Palmitic acid amount (mg)        | 100                             | 250 | 400 |
| $X_2$ : Poloxamer 407 amount(mg)         | 100                             | 200 | 300 |
| $X_3$ : Sonication time (sec)            | 10                              | 95  | 180 |
| <b>Responses</b>                         | <b>Desirability constraints</b> |     |     |
| $Y_1$ : Entrapment efficiency (%)        | Maximize                        |     |     |
| $Y_2$ : Particle size (nm)               | Minimize                        |     |     |
| $Y_3$ : Polydispersity index             | Minimize                        |     |     |
| $Y_4$ : <i>In vitro</i> release, Q8h (%) | Maximize                        |     |     |
| $Y_5$ : Dissolution efficiency (%)       | Maximize                        |     |     |

dissolution efficiency ( $Y_5$ , DE%).

The composition of each of the 17 formulae is indexed in Table 2.

The choice of the best fit model was based upon adequate precision ratio, determination coefficient ( $R^2$ ), and analysis of variance (ANOVA) to recognize the significance of the model and the consequences of each factor at  $P \leq 0.05$ .

Adequate precision  $>4$ , narrow gap difference between adjusted and predicted  $R^2$ , and insignificant lack of fit propose the power of the model to pilot the experimental design space.

Design-Expert®7 software was used to generate 3D, contour, and interaction plots for each response to study the effect of each factor and show up the interaction between them.

#### 2.2.4. Preparation of ZP-loaded NLCs

ZP-loaded NLCs were formulated by hot emulsification-ultrasonication method (Ali et al., 2022). In all formulations, the overall lipid phase concentration remained constant at 10%w/v. Briefly certain amounts of palmitic acid and cod liver oil were heated to 70 °C (exceeding the melting point of solid lipid with 5 °C), then drug solution (5 mg/mL) in acetone was added up to the molten lipid. The mixture was then magnetically stirred till clear. The aqueous phase composed of different PLX 407 amounts dissolved in distilled water was then heated to an equivalent temperature of the lipid phase and added dropwise to the melted lipid under magnetic heating stirring (WiseStir, Daihan Scientific Company, Daihan, Chhattisgarh, India) at 1200 rpm for 10 min. The formed dispersion was then sonicated utilizing a probe-type sonicator at 60 W (Probe Sonicator Ultrasonic Processor model VCX 750, Newtown, CT) while placed in an ice bath to avoid excessive heating caused by probe sonication. Finally, the prepared systems were kept in an ice bath for 15 min allowing solidification of the developed NLCs. The resultant formulations were preserved at 4 °C for further investigations. All formulations were prepared in triplicates to ensure reproducibility.

#### 2.2.5. In vitro characterization of prepared ZP-loaded NLCs

**2.2.5.1. Determination of entrapment efficiency (EE %).** ZP-loaded NLCs suspensions were ultracentrifuged at 15,000 rpm at 4 °C  $\pm$  2 using an ultra-cooling centrifuge (Model 8880, Centurion Scientific Ltd., W. Sussex, UK). The supernatant was thrown away, then the separated NLCs were washed twice using distilled water and re-centrifuged. The prepared NLCs were then dissolved in methanol (Al-Attas et al., 2017) by sonication for 5 min. Entrapped ZP amount was then determined spectrophotometrically at  $\lambda_{max} = 304$  nm (Zhou et al., 2020) by using an appropriate calibration curve of pure ZP in methanol, EE% is calculated as follows, Eq. 1:

$$EE\% = \frac{\text{amount of entrapped ZP}}{\text{total amount of ZP}} \times 100$$

**2.2.5.2. Determination of particle size, zeta potential, and polydispersity index.** Zetasizer Nano ZS (Malvern Instruments Ltd., Worcestershire, UK) was used to assess particle size, zeta potential, and polydispersity index (PDI) at 25 °C and refractive index of 1.330. Samples were prepared by 10 times dilution using distilled water to produce a proper uniform dispersion with good scattering intensity (Joseph Naguib et al., 2020). All samples were measured in triplicates to ensure reproducibility.

**2.2.5.3. In vitro drug release.** In vitro drug release patterns were recorded utilizing the dialysis bag method which is the most common method used for in vitro drug release screening from colloidal drug carriers (Moreno-Bautista and Tam, 2011). A volume of NLCs corresponding to 5 mg ZP was added in the dialysis bag, previously soaked overnight in phosphate buffer saline (PBS) at pH equals 6.4 (Nour et al., 2016), then the bag was dipped in 100 mL of PBS (pH = 6.4) containing 1% w/v Tween 80 to attain sink conditions placed in amber-colored glass bottles because of ZP light sensitivity (Terblanche et al., 2000). The bottles were

**Table 2**

The composition and the measured responses of the central composite face-centered design (CCFD) for preparation of ZP-NLCs.<sup>a,b,c</sup>

| Formula code            | Formulations Independent variables Responses |                |                |                  |                    |                  |                   |                  |                  |
|-------------------------|--|----------------|----------------|------------------|--------------------|------------------|-------------------|------------------|------------------|
|                         | Y <sub>1</sub>                               | Y <sub>2</sub> | Y <sub>3</sub> | Y <sub>4</sub>   | Y <sub>5</sub>     |                  |                   |                  |                  |
|                         | X <sub>1</sub>                               | X <sub>2</sub> | X <sub>3</sub> | EE (%)           | PS (nm)            | PDI              | * ZP (mV)         | Q8 h (%)         | DE (%)           |
| <b>Factorial points</b> |  |                |                |                  |                    |                  |                   |                  |                  |
| NLC-1                   | 100  | 100            | 10             | 95.90 $\pm$ 2.05 | 70.11 $\pm$ 20.76  | 0.17 $\pm$ 0.02  | -25.50 $\pm$ 2.83 | 92.37 $\pm$ 3.44 | 91.24 $\pm$ 1.36 |
| NLC-2                   | 400  | 100            | 10             | 70.60 $\pm$ 2.97 | 153.88 $\pm$ 18.39 | 0.37 $\pm$ 0.13  | -24.75 $\pm$ 3.04 | 47.59 $\pm$ 3.13 | 79.48 $\pm$ 2.52 |
| NLC-3                   | 100  | 300            | 10             | 98.01 $\pm$ 0.98 | 55.60 $\pm$ 23.28  | 0.07 $\pm$ 0.02  | -27.75 $\pm$ 3.39 | 77.53 $\pm$ 1.37 | 86.84 $\pm$ 3.28 |
| NLC-4                   | 400  | 300            | 10             | 78.52 $\pm$ 4.21 | 120.80 $\pm$ 41.41 | 0.45 $\pm$ 0.28  | -29.4 $\pm$ 4.81  | 43.52 $\pm$ 3.85 | 78.26 $\pm$ 5.18 |
| NLC-5                   | 100  | 100            | 180            | 93.50 $\pm$ 4.53 | 68.20 $\pm$ 27.81  | 0.14 $\pm$ 0.03  | -33.05 $\pm$ 4.03 | 78.89 $\pm$ 2.86 | 87.76 $\pm$ 2.77 |
| NLC-6                   | 400  | 100            | 180            | 65.12 $\pm$ 4.81 | 122.30 $\pm$ 12.88 | 0.42 $\pm$ 0.11  | -32.20 $\pm$ 4.53 | 51.51 $\pm$ 4.65 | 77.37 $\pm$ 1.12 |
| NLC-7                   | 100  | 300            | 180            | 92.00 $\pm$ 3.54 | 53.20 $\pm$ 14.24  | 0.13 $\pm$ 0.03  | -32.80 $\pm$ 5.66 | 76.87 $\pm$ 3.80 | 85.96 $\pm$ 2.01 |
| NLC-8                   | 400  | 300            | 180            | 76.66 $\pm$ 4.40 | 104.51 $\pm$ 41.23 | 0.40 $\pm$ 0.12  | -34.10 $\pm$ 4.86 | 44.21 $\pm$ 1.40 | 79.36 $\pm$ 2.12 |
| <b>Axial points</b>     |  |                |                |                  |                    |                  |                   |                  |                  |
| NLC-9                   | 100  | 200            | 95             | 97.32 $\pm$ 1.16 | 59.24 $\pm$ 23.88  | 0.01 $\pm$ 0.01  | -29.70 $\pm$ 5.57 | 63.18 $\pm$ 1.87 | 84.97 $\pm$ 0.33 |
| NLC-10                  | 400  | 200            | 95             | 75.60 $\pm$ 3.11 | 120.00 $\pm$ 17.07 | 0.43 $\pm$ 0.05  | -31.50 $\pm$ 2.83 | 34.94 $\pm$ 4.17 | 74.63 $\pm$ 2.64 |
| NLC-11                  | 250  | 100            | 95             | 90.93 $\pm$ 6.24 | 94.84 $\pm$ 13.34  | 0.29 $\pm$ 0.14  | -32.50 $\pm$ 3.61 | 34.33 $\pm$ 3.07 | 73.99 $\pm$ 0.98 |
| NLC-12                  | 250  | 300            | 95             | 92.20 $\pm$ 3.82 | 84.60 $\pm$ 44.38  | 0.18 $\pm$ 0.03  | -33.51 $\pm$ 4.81 | 39.90 $\pm$ 0.42 | 76.26 $\pm$ 3.51 |
| NLC-13                  | 250  | 200            | 10             | 91.17 $\pm$ 4.50 | 91.80 $\pm$ 32.69  | 0.29 $\pm$ 0.23  | -26.70 $\pm$ 3.11 | 42.92 $\pm$ 2.80 | 76.36 $\pm$ 3.03 |
| NLC-14                  | 250  | 200            | 180            | 93.65 $\pm$ 4.31 | 82.11 $\pm$ 33.01  | 0.27 $\pm$ 0.13  | -33.40 $\pm$ 4.10 | 46.04 $\pm$ 2.06 | 77.30 $\pm$ 1.27 |
| <b>Center points</b>    |  |                |                |                  |                    |                  |                   |                  |                  |
| NLC-15                  | 250  | 200            | 95             | 92.63 $\pm$ 2.87 | 86.10 $\pm$ 13.39  | 0.09 $\pm$ 0.03  | -32.55 $\pm$ 4.31 | 39.49 $\pm$ 2.67 | 76.08 $\pm$ 1.58 |
| NLC-16                  | 250  | 200            | 95             | 92.00 $\pm$ 4.95 | 86.10 $\pm$ 24.74  | 0.09 $\pm$ 0.03  | -33.55 $\pm$ 5.66 | 39.49 $\pm$ 2.39 | 75.95 $\pm$ 2.83 |
| NLC-17                  | 250  | 200            | 95             | 93.00 $\pm$ 4.95 | 84.33 $\pm$ 20.10  | 0.32 $\pm$ 0.14  | -33.05 $\pm$ 3.61 | 47.60 $\pm$ 3.96 | 77.37 $\pm$ 1.12 |
| NLC-OP                  | 100  | 116.56         | 10             | 2.44 $\pm$ 94.31 | 13.57 $\pm$ 71.76  | 0.097 $\pm$ 0.15 | -25.71 $\pm$ 2.69 | 83.89 $\pm$ 1.77 | 88.63 $\pm$ 2.01 |

X<sub>1</sub>: Palmitic acid amount (mg).

X<sub>2</sub>: Poloxamer 407 amount (mg).

X<sub>3</sub>: Sonication time (sec).

<sup>a</sup> All formulae are prepared by using 25 mg zopiclone.

<sup>b</sup> All data are presented as mean  $\pm$  SD; n = 3.

<sup>c</sup> Fixed amount of cod liver oil (liquid lipid) is added in all formulae.

\* ZP: Zeta potential.

then positioned in a thermostatically controlled shaker (Unimax, IKA, Germany) at 100 rpm at a temperature equal to  $37 \pm 0.2$  °C. At pre-defined time intervals, three mLs of the release medium were withdrawn (0.5, 1, 2, 4, 6, 8 h). To keep sink conditions, a fresh release medium is immediately added to replace the withdrawn sample. Samples were then analyzed for ZP content spectrophotometrically at  $\lambda_{\max} = 304$  nm. ZP solution underwent the same procedure to check if the dialysis membrane had any effect on the retardation of drug passage through the utilized dialysis bag. Drug dissolution efficiency (DE%) was also calculated, where DE% was the area under the release curve designated as the % of the area of the rectangle representing 100% release at the exact time point. The following equation was employed in calculating DE% (Khan and CT, 1972; Nour et al., 2016), Eq. 2:

$$DE\% = \int_0^t \frac{y}{y_{100}} dt \times 100$$

where the integral symbolizes the area under the release curve to time  $t$ , and  $y_{100}$  is the rectangle area expressing 100% release at the same time.

The data from drug release profiles data were tailored to zero, first and Higuchi diffusion models. The model with the highest  $R^2$  reflects the adopted release mechanism.

**2.2.5.4. Desirability and optimization.** Optimization of the composition of the prepared ZP-loaded NLCs was set by applying numerical optimization and desirability function. The goal was to create NLCs with maximized EE%, *in vitro* drug release percentage, and DE% and minimized PS and PDI. Desirability function is a tool to determine the optimum measure for independent variables by first, evaluating the desirability index for each response, and then merging all response variables into a single desirability function ranging from 0 to 1 to describe the superior values of the independent parameters. (Mani and Ebrahimi, 2022; Naguib et al., 2020).

## 2.2.6. Characterization of the optimized ZP-loaded NLCs

**2.2.6.1. Morphological visualization.** The shape, uniformity, and degree of aggregation were imaged by transmission electron microscope (TEM) (JEM-1230, Jeol, Tokyo, Japan). The optimized formula (NLC-OP) was diluted with distilled water then 5  $\mu$ L was put on carbon-coated 400-mesh copper grids. The grid was then treated with a drop of filtered 2% phosphotungstic acid (PTA stain), pH 7, and left to stain for 30–60 s and then examined under TEM (Medina-Montano et al., 2022).

**2.2.6.2. Fourier transform infrared (FT-IR) spectroscopy.** Bruker FTIR spectrometer (Model 22; Bruker, Coventry, UK) was utilized to study any possible interactions between ZP and components used in the formulation. Samples of ZP, palmitic acid, cod liver oil, PLX 407, and lyophilized optimized NLCs (NLC-OP) formula (NLC-OP was frozen and then lyophilized at  $-45$  °C under  $7 \times 10^{-2}$  mbar pressure utilizing a lyophilizer; Novalyph-NL 500, Savant Instruments, Holbrook, NY) were mixed with KBr pellets and was studied in transmission mode with wave numbers ranging from 4000 to 400  $\text{cm}^{-1}$ .

**2.2.6.3. Ex vivo cytotoxicity assessment.** To reveal any cytotoxic effect of the optimized ZP-loaded NLCs (NLC-OP) as any sign of alteration or pathological damage to the nasal mucosa, an *ex vivo* cytotoxicity study was conducted. Isolated sheep nasal mucosa is believed to have a morphology and histology almost identical to human nasal mucosa (Shaghilil et al., 2022). Thus, a 2-year-old sheep's head was obtained from a nearby slaughterhouse. (Cairo, Egypt). After creating a longitudinal excision in the lateral walls of the nose away from the septum to expose the nasal cavity, the nasal mucosa from the anterior and posterior sections was meticulously isolated from the sheep (Gerber et al., 2022). Immediately after isolation the nasal mucosa was washed to remove any adhesive or connective tissues (Gadhav et al., 2021), then

immersed in ice-cold PBS pH 6.4 (Nagaraja et al., 2021). Fragments from both anterior and posterior divisions of the nasal mucosa were obtained. After that, each fragment was divided into three pieces. At random, segments were allocated into three groups. Group I was treated with PBS pH 6.4 (negative control) (Mahajan and Patil, 2021), Group II was treated with isopropyl alcohol (positive control) (Kumbhar et al., 2021), and Group III was treated with the optimized NLC-OP formula. Each group was exposed to the same volumes (2 mL) of the treatments. Fragments were left in the treatments for 2 h. Subsequently, they were rinsed with distilled water and stored in a saline solution containing formalin at 10% concentration (Verekar et al., 2020).

After clearing in xylene, the samples were embedded in paraffin in a hot oven at 56 °C for 24 h. Prepared paraffin blocks were eventually cut by the means of a sledge microtome into 4  $\mu$ m thickness units. The obtained slices were placed on a glass slide, deparaffinized, tinted with hematoxylin and eosin (H&E), and examined under a light microscope (National model 138, China) (El-Dahmy et al., 2021; Naguib et al., 2020).

## 2.2.7. In vivo biodistribution of the optimized formula

Biodistribution in mice was evaluated by one of the radiobiological techniques using radioiodinated ZP in different formulations.

**2.2.7.1. Formulation of radioiodinated ZP.** Formulation of [ $^{131}$ I]iodo-ZP was carried out by studying many parameters which are Chloramine-T (CAT) concentration, ZP concentration, pH value, and reaction time. ZP and CAT were freshly prepared in a concentration of 5 mg/mL using acetone as a solvent. Then, predetermined volumes from ZP solutions containing different amounts (0.125–4 mg) of ZP were placed in dark stoppered reaction glass vials. Secondly, definite volumes of CAT with amounts (50–500  $\mu$ g) were added to ZP glass vials. Subsequently, [ $^{131}$ I] NaI was added. Lastly, the pH was set to the desired value and the reaction volume was finalized to 1 mL. After certain reaction times, the reaction was terminated using 5  $\mu$ L of sodium thiosulfate (190 mM) (Ibrahim et al., 2018). The reaction was monitored via a chromatographic technique using chloroform: methanol (9:1) as a mobile phase and the radiolabeling efficiency % (RE%) was also determined by the same technique, where the iodinated compound migrates at  $R_f = 0.7$  to 1.00 while the free iodide remains at the origin at  $R_f = 0.00$ .

**2.2.7.2. Radio formulation of [ $^{131}$ I]iodo-ZP-NLCs.** [ $^{131}$ I]iodo-ZP-NLCs were prepared by the same procedure mentioned before but using [ $^{131}$ I]iodo-ZP instead of ZP and the final dispersion was sonicated at the same temperature of 70 °C using a bath sonicator for 5 min. Finally, it was mixed by magnetic stirrer in an ice bath at 300 rpm for 15 min allowing solidification of nanoparticles. The radiolabeling efficiency % of [ $^{131}$ I]iodo-ZP-NLCs was reassessed by chromatographic technique to confirm the *in vitro* stability of formulated [ $^{131}$ I]iodo-ZP-NLCs.

**2.2.7.3. Animal study.** The protocol of animal experimentation was consulted and approved by the Research Ethics Committee of Faculty of Pharmacy, Cairo University, Egypt (REC-FOPCU) with a reference number of PI (2351). Procedures for biological investigations followed the criteria established by the Egyptian Atomic Energy Authority (EAEA) Committee, Cairo, Egypt (no. 216/2022).

A biodistribution study of optimized [ $^{131}$ I]iodo-ZP-NLCs was used to assess the *in vivo* behavior of the optimized ZP-loaded NLCs (NLC-OP) in fifty-four male Swiss albino mice weighing 20–25 g. On the day of the experiment, mice were divided into three groups of 18 mice each. (Fahmy et al., 2018).

The preparations administration was as follows:

Group I: intranasal (IN) [ $^{131}$ I]iodo-ZP drug solution (DS)

Group II: intranasal (IN) [ $^{131}$ I]iodo-ZP-NLCs

Group III: intravenous (IV) [ $^{131}$ I]iodo-ZP-NLCs via mice tail vein

Every mouse was administrated a volume containing ZP dose

corresponding to 7.5 µg/g body weight and 30 MBq of radioactivity. Intranasal (IN) administration was done into the nostrils of each mouse with the aid of a Hamilton syringe coupled to a 0.1 mm internal diameter polyethylene tubing at the delivery point (El-Setouhy et al., 2016). Throughout the administration, animals were gently positioned from the back in an inclined position to permit them to breathe the solution.

At predetermined time intervals (5 min, 0.25, 0.5, 1, 2, and 4 h post-delivery) (Fahmy et al., 2018), three mice were sacrificed from each group.

The blood samples were withdrawn by cardiac puncture, other organs including the brain were separated and cleaned of any sticky tissue or fluid, washed using normal saline, weighed, and their radioactivity due to [<sup>131</sup>I]iodo-ZP uptake was measured utilizing a NaI (Tl) γ-ray scintillation counter. Since it was very difficult to isolate all bones, muscles, and blood of mice, they were considered to be 10, 40, and 7% of the total body weight. (Motaleb et al., 2011; Shamsel-Din and Ibrahim, 2017), respectively. The sample of muscles, bones, and blood is weighed and the total weight of each of them is calculated. The percentage of the injected dose per gram (tissue, fluids, or organ) (% ID/g) at the pre-determined periods in a group comprising three mice was calculated by using the equation below (Sakr et al., 2017), Eq. 3:

$$\%ID/g = \frac{\text{Activity of tissue or fluid or organ} \times 100}{\text{Total injected activity} \times \text{Weight of tissue or fluid or organ}}$$

For each mouse, the pharmacokinetic parameters of all ZP formulations were defined, encompassing maximal [<sup>131</sup>I]iodo-ZP uptake (% ID/g) (blood or brain), C<sub>max</sub>, as well as T<sub>max</sub>. Kinetic-2000 software has been used to determine the area under the concentration-time graphs from zero to four hours (AUC<sub>0-4</sub> h%ID/g) and from zero to infinity

(AUC<sub>0-∞</sub> h%ID/g) (Innaphase, Philadelphia, PA, USA).

Relative bioavailability for intranasal NLCs created with [<sup>131</sup>I]iodo-ZP versus [<sup>131</sup>I]iodo-ZP solution was estimated by implementing the next equation (Serralheiro et al., 2014), Eq. 4:

$$\text{Relative bioavailability}\% = \frac{(AUC_{NLCs0-\infty})_{IN}}{(AUC_{solution0-\infty})_{IN}} \times 100$$

Drug targeting efficiency (DTE) (Zhao et al., 2007), drug targeting index (DTI) (Abo El-Enin et al., 2022), and direct transport percentage (DTP) may all be used to describe NLC-OP capability to target the brain following intranasal delivery (Sayyed et al., 2022). DTE% is the averaged distribution ratio of the medication amidst brain and blood, and it is determined using the equation below. Eq. 5:

$$DTE\% = \frac{AUC_{brain\ IN}}{AUC_{blood\ IN}} \times 100$$

DTI values were got from the following equation, Eq. 6:

$$DTI = \frac{(AUC_{brain}/AUC_{blood})_{IN}}{(AUC_{brain}/AUC_{blood})_{IV}}$$

Here AUC<sub>brain</sub> reflects the area under the concentration vs time plot from zero to four hours for ZP in brain and AUC<sub>blood</sub> represents the area under the concentration vs time graph from zero to four hours corresponding to ZP in blood.

The following equation is used to calculate DTP%, which represents the proportion of medication directly delivered to the brain via the olfactory and trigeminal routes, Eq. 7:

$$DTP\% = \frac{B_{IN} - B_X}{B_{IN}} \times 100$$

Whereas B<sub>IN</sub> is the entire brain AUC<sub>0-4</sub> after intranasal administration and B<sub>X</sub> is a portion of the systemic circulation's brain AUC<sub>0-4</sub> upon intranasal administration, it was determined as stated by the following equation, Eq. 8:

$$B_X = \frac{B_{IV}}{P_{IV}} \times P_{IN}$$

Where B<sub>IV</sub> is the brain AUC<sub>0-4</sub> succeeding intravenous administration, P<sub>IV</sub> is the blood AUC<sub>0-4</sub> after intravenous administration and P<sub>IN</sub> is the blood AUC<sub>0-4</sub> following intranasal administration.

### 3. Results and discussion

#### 3.1. Preliminary trials

##### 3.1.1. Selection of solid lipid

To find out if there was a significant difference between the solubility of ZP in different lipids, a one-way analysis of variance (ANOVA) was used. Higher significant solubility of ZP was found in PA (88 mg% ± 5.6) with a p value equal to 0.0001 (Fig. 1). Therefore PA was chosen for NLCs formulation. Besides, PA has a melting point of -63°C which is suitable for NLCs formulation to ensure that it will remain in a solid state in the body and at room temperature.

##### 3.1.2. Selection of surfactant

Three surfactants namely Tween 80, PLX 407, and polyoxyl 40 -all with HLB value >12 which is better for stabilizing o/w emulsions- were selected for screening. Poloxamer 407 had the lowest PS of 111 ± 6.9 nm (p = 0.0001) and the highest EE% of 78.29% ± 2.7 at a p value of 0.0034 (Fig. 2), therefore it was nominated for further NLCs preparation after testing of significance by one-way ANOVA.

#### 3.2. Characterization of the developed ZP-loaded NLCs

##### 3.2.1. Effect of independent factors on EE%

Table 2 displays the EE% of ZP in all ZP-loaded NLCs. THE EE% of all formulae ranged from 65.12% ± 4.81 (NLC-6) to 98.01% ± 0.98 (NLC-3). The model was significant (p < 0.0001) in an ANOVA test for the influence of independent factors on the EE% of ZP-NLCs predicated on a quadratic model with an adequate precision of 24.268, also adjusted R<sup>2</sup> (0.9723) came to an acceptable accord with the predicted R<sup>2</sup> (0.8907) Table 3. The lack of fit was insignificant (p > 0.05) denoting the precision of statistical outcomes. ANOVA analysis showed that factors X<sub>1</sub> and X<sub>3</sub> had a negative significant effect whereas factor X<sub>2</sub> had a positive effect as represented in the final equation by means of coded factors as follows:

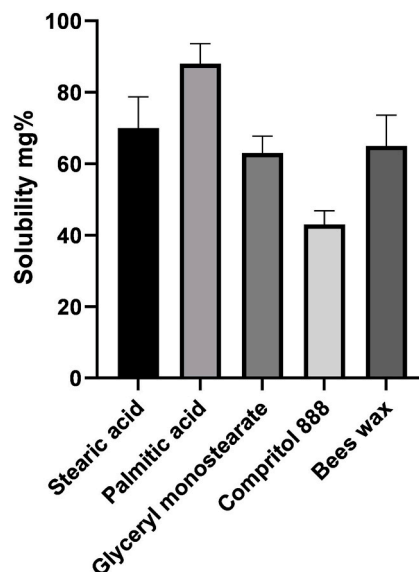


Fig. 1. The solubility of Zopiclone in different solid lipids.

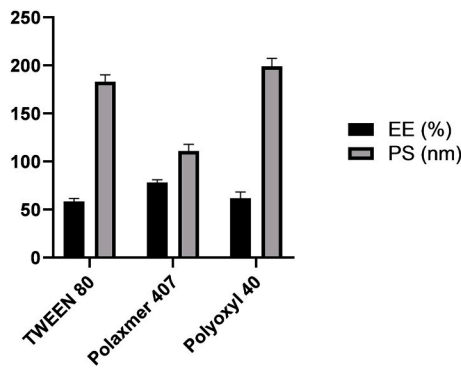


Fig. 2. Entrapment efficiency and particle size obtained using different surfactants.

$$EE\% = 92.23 - 11.02X_1 + 2.13X_2 - 1.33X_3 + 2.36 X_1X_2 - 7.09X_1^2$$

Considering factor  $X_1$ ; PA amount, increasing solid lipid amount was accompanied with a decrease in the EE% (Fig. 3A). As mentioned earlier the main goal of the production of NLCs as the second generation of SLNs is to increase drug loading and encapsulation by the addition of a liquid lipid which creates less ordered crystal lattice resulting in more voids and deformations which accommodate a higher percentage of the drug (Apostolou et al., 2021). Thus increasing solid lipid amount in NLCs will subsequently decrease EE%. This is harmonious with the results generated by Makoni et al. (Makoni et al., 2019) when comparing the EE% of both Efavirenz-loaded SLNs and NLCs where the prepared NLCs resulted in higher EE %. Also, hydrochlorothiazide-loaded NLCs prepared by Mura et al. (Mura et al., 2021) showed higher EE% than the corresponding SLNs. The same effect was reported by Dolatabadi et al. (Dolatabadi et al., 2021).

Table 3

Regression analysis of the observed responses according to the best fitting model.

| Response                 | Model     | R <sup>2</sup> | Adjusted R <sup>2</sup> | Predicted R <sup>2</sup> | Adequate precision | Significant terms  |
|--------------------------|-----------|----------------|-------------------------|--------------------------|--------------------|--|
| Y <sub>1</sub> : EE(%)   | Quadratic | 0.9879         | 0.9723                  | 0.8907                   | 24.268             | X <sub>1</sub> , X <sub>2</sub> , X <sub>3</sub> , X <sub>1</sub> X <sub>2</sub> , X <sub>1</sub> <sup>2</sup> |
| Y <sub>2</sub> : PS (nm) | Quadratic | 0.9931         | 0.9842                  | 0.9040                   | 36.752             | X <sub>1</sub> , X <sub>2</sub> , X <sub>3</sub> , X <sub>1</sub> X <sub>3</sub>                               |
| Y <sub>3</sub> : PDI     | Linear    | 0.7477         | 0.6895                  | 0.6427                   | 8.885              | X <sub>1</sub>   |
| Y <sub>4</sub> : Q8h (%) | Quadratic | 0.9458         | 0.9013                  | 0.8384                   | 13.942             | X <sub>1</sub> , X <sub>1</sub> <sup>2</sup> , X <sub>3</sub> <sup>2</sup>                                     |
| Y <sub>5</sub> : DE (%)  | Quadratic | 0.9644         | 0.8690                  | 0.7963                   | 11.984             | X <sub>1</sub> , X <sub>1</sub> <sup>2</sup>   |

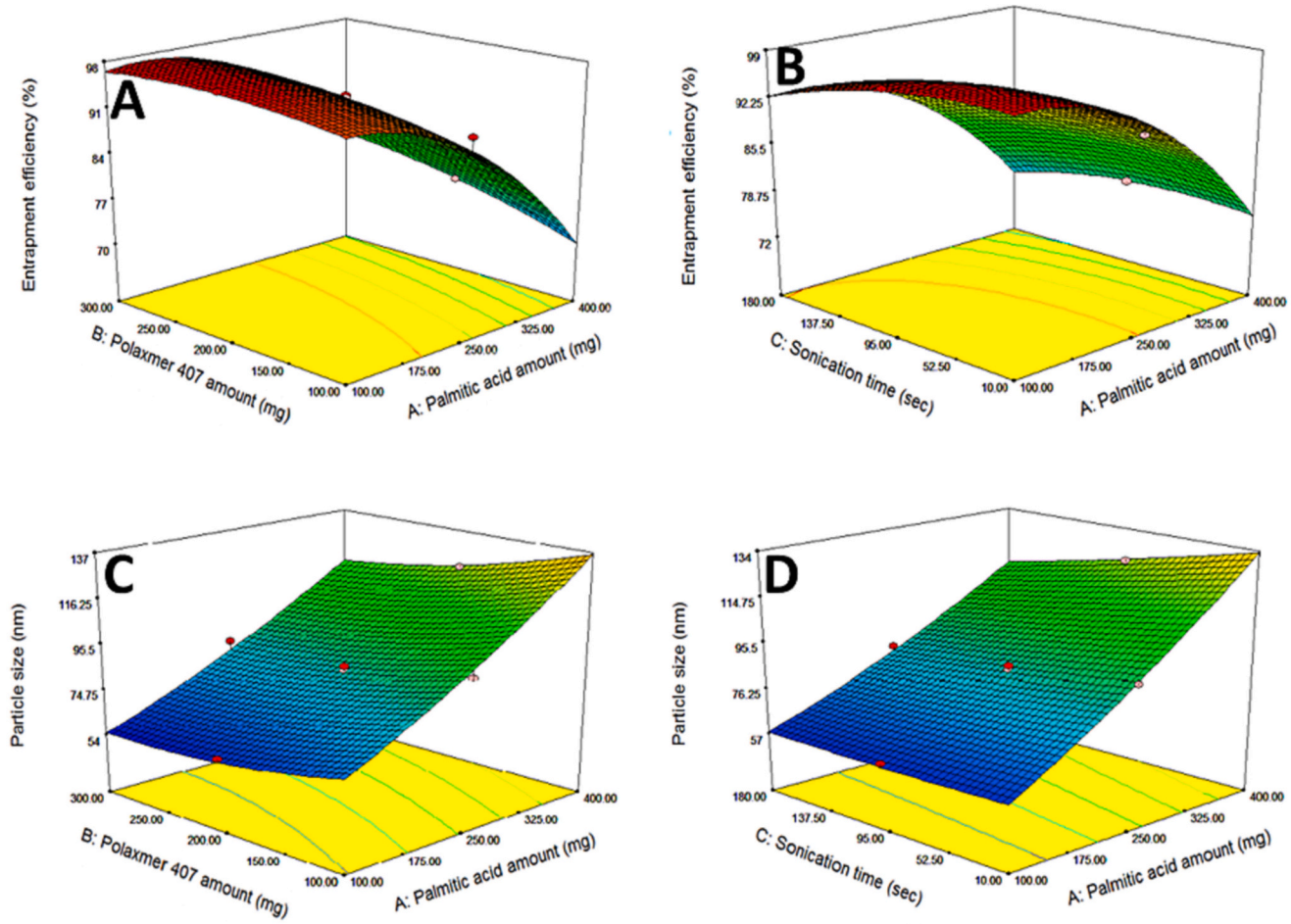


Fig. 3. Three-dimensional response surface plots typifying the effect of the significant factors and interactions between them on the responses of ZP-loaded NLCs; The effect of palmitic acid and poloxamer 407 amounts (mg) on entrapment efficiency (A), The effect of palmitic acid (mg) and sonication time (sec) on entrapment efficiency (B), The effect of palmitic acid and poloxamer 407 amounts (mg) on particle size (C), The effect of palmitic acid (mg) and sonication time (sec) on particle size (D).

Regarding factor  $X_2$ ; PLX407 amount, increasing PLX 407 amount significantly increased the EE% (Fig. 3A). PLX 407 is a triblock copolymer that consists of polyethylene oxide (hydrophilic part) and polypropylene oxide (hydrophobic part). This difference in hydrophobicity allows their orientation to form micelles in the aqueous phase (Thapa et al., 2020). Thus forming a rigid layer of surfactant around the formed particles, preventing drug leaking and offering better drug housing and so better drug EE% (Abdelhakeem et al., 2021). These results came in agreement with the results found by Zafar et al. (Zafar et al., 2022) who prepared NLCs-based erythromycin gel and revealed that the increase of Pluronic F127 (poloxamer 407) from 2% to 5% was accompanied by an increase in EE %. The positive effect of surfactants on EE% was also reported by Gadhave et al. (Gadhave and Kokare, 2019) and Kataria et al. (Kataria et al., 2022).

Concerning factor  $X_3$ , increasing sonication time would in turn increase the breakdown of lipid particles and subsequent escape of the drug from NLCs and eventually decreasing the EE% (Fig. 3B). The negative effect of increasing sonication time on EE % was similarly reported after piperine NLCs formulation (Zafar et al., 2021). Also, comparable results were declared by Agrawal et al. (Agrawal et al., 2022) who found that EE% of entacapone in the formulated NLCs decreased with increasing sonication time.

### 3.2.2. Effect of independent factors on particle size

Decreasing particle size is crucial for nose-to-brain delivery to facilitate BBB permeation. The measured PS of the prepared formulae ranged from 53.2 nm  $\pm$  14.24 (NLC-7) to 153.88 nm  $\pm$  18.39 (NLC-2) as shown in Table 2. ANOVA test for the consequence of independent variables on the PS of ZP-NLCs based on quadratic model showed that the model was significant ( $p < 0.0001$ ) with high adequate precision (36.752) and a narrow gap between adjusted  $R^2$  (0.9842) and the predicted one (0.9040) (Table 3). The lack of fit was insignificant ( $p > 0.05$ ) exhibiting statistical accuracy. ANOVA analysis showed that factor  $X_1$  (solid lipid amount) had a positive significant effect on PS (Fig. 3C), whereas both factors  $X_2$  (PLX 407 amount) (Fig. 3C) and  $X_3$  (sonication time) had a negative significant effect (Fig. 3D) This was further confirmed by the final equation as a combination of coded factors as follows:

$$PS = 90.45 + 31.51X_1 - 9.06X_2 - 6.19X_3 - 5.45X_1X_3$$

The effect of factor  $X_1$  (PA amount) could be assigned to the verity that increasing solid lipid amounts resulted in a higher viscosity of the formed dispersion which by extension led to larger PS while formulae with higher liquid lipid content had lower viscosity and thus smaller PS. These findings are consistent with the work of Singh et al. (Singh et al., 2021) where the formulation of mupirocin-loaded NLCs with higher liquid lipid content resulted in smaller particle size. The same influence of the amount of solid lipid on NLCs particle size was recorded by de Souza et al. (de Souza et al., 2019) and Sanad et al. (Sanad et al., 2010) indicating that the mean PS of the prepared lipid nanoparticles was greatly affected by solid lipid amount and viscosity of the oil phase.

As for factor  $X_2$  (PLX407 amount), lipid nanoparticles were created using an oil-in-water (o/w) emulsification approach. Hydrophilic surfactants (HLB > 12) were examined for their superior emulsification effectiveness over lipophilic surfactants with HLB < 12. Surfactant concentration exhibited a counter effect on PS, where increasing the concentration led to the production of nanoparticles with smaller PS as it led to a reduction of the surface tension among lipid particles and the aqueous phase, in addition to the prevention of particle agglomeration (Houacine et al., 2020; Wu et al., 2021). Concerning factor  $X_3$  (sonication time), increasing sonication time led to decreasing in PS. This could be explained on the basis that ultra-sonic waves led to the breakdown of the formed particles due to high mechanical shear forces (Babazadeh et al., 2017; Mahmood et al., 2021).

### 3.2.3. Effect of independent factors on PDI

PDI is a measure of how far particles are distributed homogeneously throughout the sample, which is very important for the stability of the prepared nanoparticles. Values of PDI closer to 0 assure the homogeneity of the prepared dispersion while values closer to 1 indicates a wide range of size populations within the sample (Danaei et al., 2018; Naguib et al., 2021). All prepared formulae showed PDI values extending from  $0.01 \pm 0.01$  (NLC-9) to  $0.45 \pm 0.28$  (NLC-4) as presented in Table 2 which indicated the uniformity of the prepared NLCs. The ANOVA test for the influence of independent variables on the PDI of ZP-NLCs using a linear model revealed that the model was significant with a  $p$  value of 0.0003 and 8.885 adequate precision with a modest difference between adjusted (0.6895)  $R^2$  and predicted  $R^2$  (0.6427) (Table 3). The lack of fit was insignificant ( $p > 0.05$ ), signifying that the statistical results were precise. ANOVA analysis showed that factor  $X_1$  had a significant positive effect on PDI (Fig. 4A). Whereas factors  $X_2$  and  $X_3$  had an insignificant effect as shown in the final equation as a function of coded factors as follows:

$$PDI = 0.24 + 0.15X_1 - 0.016X_2 + 1.000E - 003X_3$$

Increasing the amount of the solid lipid used ( $X_1$ , PA amount) led to an increase in PDI values. These results come in harmony with the previously observed results by Khan et al. (Khan et al., 2021) where decreasing solid lipid: liquid lipid ratio from 9:1 to 6:4 in miltefosine-loaded NLCs preparation was accompanied by a significant decrease in PDI. Similarly, Cunha et al. (Cunha et al., 2020) reported a positive linear correlation between solid lipid ratio and PDI in the process of analysis and optimization of rivastigmine-loaded NLCs.

### 3.2.4. Effect of independent factors on zeta potential

Zeta potential refers to the extent of charge on the surface of the developed particles in the prepared mixture, which help in surmising the long-term stability of the preparations (Gupta et al., 2021). The greater the surface charge, the greater the repulsion between the particles and so leading to less aggregation between them (Haider et al., 2020). The results of the prepared formulae indicated that all prepared ZP-loaded NLCs had zeta potential ranging from  $-24.75 \text{ mV} \pm 3.04$  (NLC-2) to  $-34.1 \text{ mV} \pm 4.86$  (NLC-8) mV as shown in Table 2. The negative charge on the surface of NLCs is accredited to the free fatty acids in the structure of both solid and liquid lipids. These findings are comparable with those reported by other research groups (Tetyczka et al., 2017, 2019; Zhu et al., 2015). Since it is well-known that any colloidal system with zeta potential  $\geq \pm 30 \text{ mV}$  is physically stable (da Silva et al., 2022), this proves good physical stability of most of the currently prepared dispersions.

Statistical analysis utilizing ANOVA revealed the absence of a significant effect of any of the studied variables on zeta potential.

### 3.2.5. Effect of independent factors on in vitro drug release

*In vitro* percentage release of ZP from all investigated formulae, compared to the permeation of ZP solution from the dialysis bag are plotted vs. time as shown in (Fig. 5). The permeation of the ZP solution of the dialysis bag manifested fast release with >98% of ZP released in the first 2 h which assured that cellulose membrane did not have any retardation effect on ZP release and that ZP diffused freely through it without any hindrance. Drug percentage released ranged from 34.33%  $\pm$  3.07 (NLC-11) to 92.37%  $\pm$  3.44 (NLC-1). ANOVA test for the outcome of independent variables on *in-vitro* drug release (Q8h%) of ZP-NLCs based on quadratic model showed that the model was significant ( $p$  value < 0.0001) with an insignificant lack of fit ( $p > 0.05$ ), good adequate precision 13.942 and only 0.0629 difference between adjusted and predicted  $R^2$ . The effect of both factors  $X_2$  and  $X_3$  were found to be statistically insignificant where  $X_1$  had a significant negative effect on Q8h (Fig. 4B) as shown in the final equation in terms of coded factors as follows:

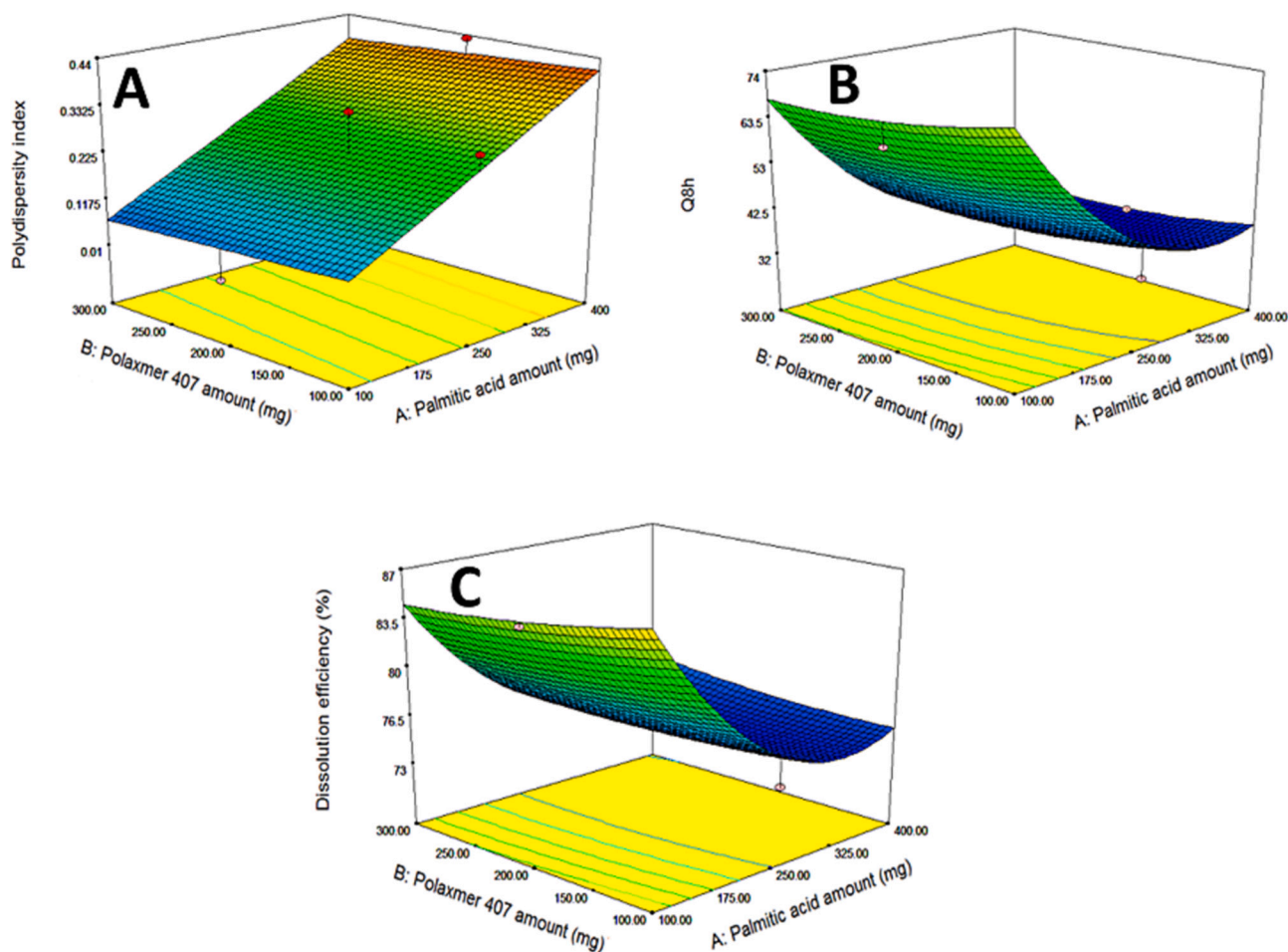


**Fig. 4.** Three-dimensional response surface plots typifying the effect of the significant factors and interactions between them on the responses of ZP-cod NLCs. The effect of palmitic acid and poloxamer 407 amounts (mg) on polydispersity index (A), The effect of palmitic acid and poloxamer 407 amounts (mg) on *in vitro* drug release after 8 h (B), The effect of palmitic acid and poloxamer 407 amounts (mg) on dissolution efficiency (C).

$$Q8h\% = 38.55 - 16.71X_1 - 2.27X_2 - 0.64X_3 + 14.51X_1^2 + 9.96X_3^2$$

The effect of factor  $X_1$ ; PA amount can be explained on basis that increasing solid lipid amount as mentioned before means more ordered crystalline lattice, which indeed caused more hindering to the diffusion path of ZP release and so decrease drug release. These results were the same as those obtained by Fathi et al. (Fathi et al., 2018) who showed that increasing the oleic acid amount as the liquid lipid in simvastatin-loaded NLCs increased the *in vitro* drug release. Likely, increasing soybean oil amount in acetone-loaded NLCs led to a higher drug release profile (Kraisit and Sarisuta, 2018).

Regarding DE%, ANOVA assessment for the effect of independent variables on the dissolution efficiency of ZP-loaded NLCs based on quadratic model showed that the model was significant  $p$  value  $< 0.0001$  with an insignificant lack of fit ( $p > 0.05$ ). Reasonable adequate precision 11.984 and a small gap between adjusted (0.8690) and predicted (0.7963)  $R^2$  demonstrating the precision of statistical results. ANOVA analysis showed that factors  $X_2$  and  $X_3$  had an insignificant effect whereas factor  $X_1$  had a negative effect (Fig. 4C) as displayed in the final equation in the form of coded factors as follows:

$$DE\% = 76.19 - 4.77X_1 - 0.32X_2 - 0.44X_3 + 6.4X_1^2$$

The negative effect of PA on DE% is a reflection to its effect on drug release where increasing solid lipid amount results in more obstruction to drug release and so lower drug DE %.

*In vitro* drug release profiles of the examined NLCs formulae were most properly fitted to Higuchi diffusion model with the highest

calculated  $R^2$  values. This indicates the erosion of the lipid matrix enabling drug diffusion into the release medium. These results are comparable with those provided by Pradhan et al. (Pradhan et al., 2021) who prepared calcipotriol-loaded NLCs for psoriasis treatment. Also comparable release profiles were conducted by Elmowafy et al. (Elmowafy et al., 2017) after formulation of atorvastatin-loaded NLCs intended for oral administration.

### 3.3. Model validation and selection of the optimized ZP-loaded NLCs candidate formula

Design of experiment is a set of mathematical techniques which is established to optimize different output responses of a certain process by several input factors (Ghelich et al., 2019). Response surface methodology (RSM) is a pivotal mathematical-statistical technique to estimate the effect of different variables on process outcomes by producing a polynomial mathematical relationship between them (Caglar et al., 2018). RSM is a non-rotatable design that requires three levels for each factor as for each surface of the factorial space, the star points are the centered ones (Bhattacharya, 2021). The main privilege of RSM over traditional methods is minimization of the number of experimental runs needed, so a faster, cost-effective, and more efficient optimization process (Samadi et al., 2020). The most fitted model for each response is adopted based on adequate precision value which is an estimate of signal-to-noise ratio. Values greater than four imply that the model can explore the experimental design space. Also maximizing the  $R^2$  value which is a statistical measurement that elucidates the ratio of variance in

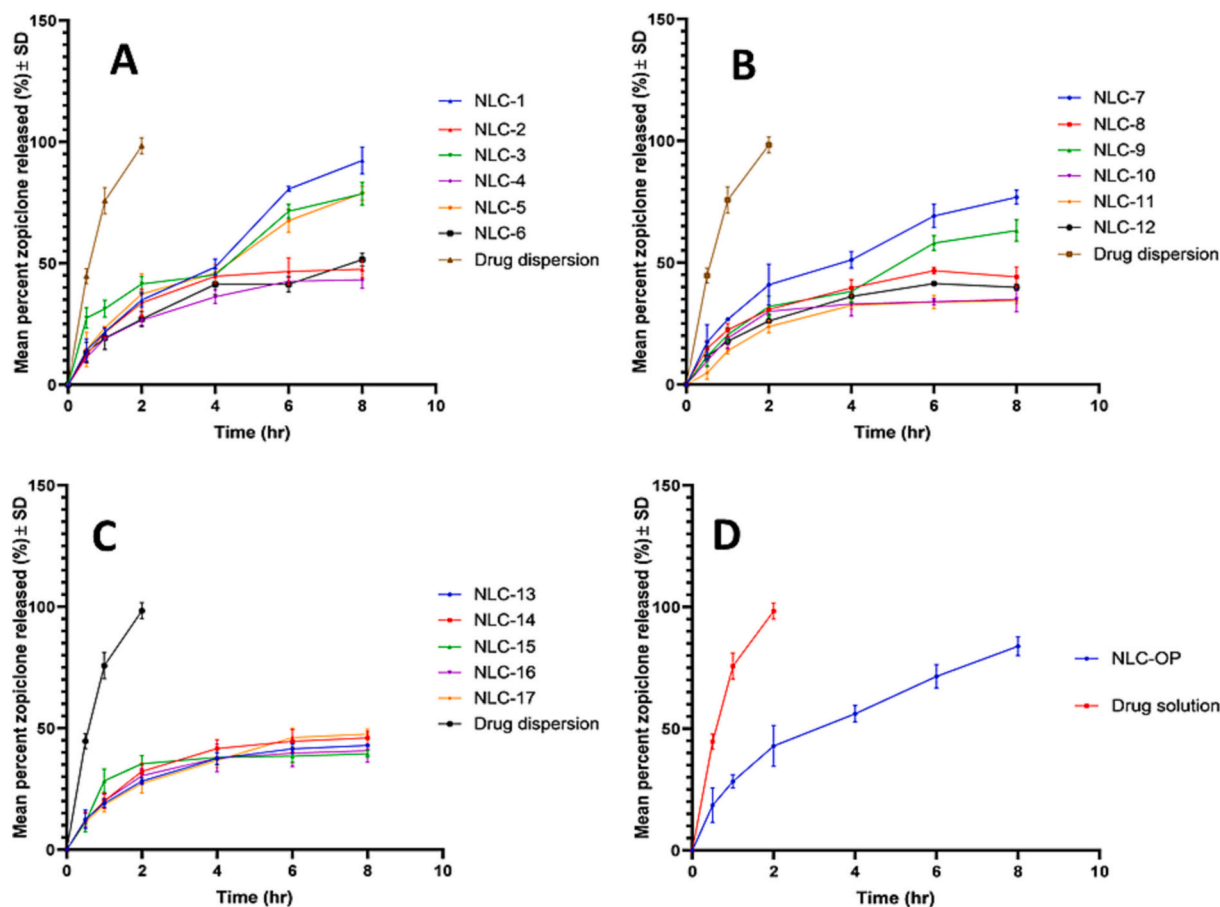


Fig. 5. *In-vitro* release profiles of the seventeen prepared formulae compared to drug solution in PBS (pH =7.4) containing 1% Tween 80 at  $37 \pm 0.5$  °C, (NLC-1 – NLC-6). (A) (NLC-7 – NLC-12). (B) (NLC-13 – NLC-17) (C) NLC-OP (D). (Results are presented as mean  $\pm$  SD, n = 3).

the dependent variable that is expounded by the independent variable (Ahmadi et al., 2005). The basis of the choice of the optimized formula was maximizing EE ( $Y_1$ , %), *in vitro* drug release ( $Y_4$ , %), and DE ( $Y_5$ , %) with minimizing PS ( $Y_2$ , nm) and PDI ( $Y_3$ ). The software recommended NLC-OP having a desirability value of 0.852. The outcome of the desirability function suggested that the optimized formula should be prepared by the following composition: 100 mg of PA and 116.56 mg PLX 407 with 10 s sonication time. The measured variables were 68.68 nm for PS, 0.097 for PDI, 94.31% for EE%, and 83.89% for Q8h with DE % equal to 88.63%. The spotted responses were asymptotic to the predicted ones with acceptable error % as shown in Table 4, substantiating the accuracy of the optimization process.

### 3.4. Characterization of the optimum NLCs formula (NLC-OP)

#### 3.4.1. Morphology of the optimized ZP-loaded NLCs formula

TEM was employed as a tool to illustrate the morphology and size of

**Table 4**  
Predicted and observed responses of optimized ZP- loaded NLCs (NLC-OP)

| Variables | Values | Responses                          | Predicted value | Actual value | Error % |
|-----------|--------|------------------------------------|-----------------|--------------|---------|
| $X_1$     | 100    | $Y_1$ : Entrapment efficiency (%)  | 96.42           | 94.31        | 2.19%   |
| $X_2$     | 116.56 | $Y_2$ : Particle size(nm)          | 68.68           | 71.27        | 3.77%   |
| $X_3$     | 10     | $Y_3$ : Polydispersity index       | 0.09            | 0.097        | 7.77%   |
|           |        | $Y_4$ : Q8h (%)                    | 80.40           | 83.89        | 4.34%   |
|           |        | $Y_5$ : Dissolution efficiency (%) | 90.19           | 88.63        | 1.73%   |

the prepared NLCs. TEM micrographs (Fig. 6) confirmed size uniformity of the prepared NLCs which appeared as spherical vesicles without any aggregation. They also displayed size that is well correlated with that obtained by the zeta sizer.

#### 3.4.2. Fourier transform infrared (FT-IR) spectroscopy

Bruker FTIR spectrometer was used to portray any likelihood of interactions between ZP and components used in the formulation. The samples of ZP, PA, cod liver oil, PLX 407, and lyophilized NLC-OP formula were investigated as shown in (Fig. 7). ZP FTIR spectra showed characteristic peaks at  $2943.37\text{ cm}^{-1}$  and  $2789.07\text{ cm}^{-1}$  corresponding to C–H bonds of the methyl group and piperazinyl ring, correspondingly. In addition, peaks were shown at  $1716.65\text{ cm}^{-1}$  corresponding to C=O of the pyrrolone ring, as well as peaks at  $1419.61\text{ cm}^{-1}$  correspondent to C–H of methylene group and  $1087.85\text{ cm}^{-1}$  corresponding to chlorine substituted aromatic ring (Abdel Razeq et al., 2018; Ming et al., 2007). Pure PA showed principle peaks at  $2916.37\text{ cm}^{-1}$  and  $2850.79\text{ cm}^{-1}$  pointing to  $-\text{CH}_2$  and  $-\text{CH}_3$  groups, respectively, in addition to peaks appeared at  $1701.22\text{ cm}^{-1}$  corresponding to C=O groups, and at  $941.26\text{ cm}^{-1}$  corresponding to the bending vibration of  $-\text{OH}$  groups (Wu et al., 2019). Cod liver oil had two characteristic peaks; one for  $-\text{C}-\text{H}$  ( $\text{CH}_2$ ) group stretching vibrations at  $2924.09\text{ cm}^{-1}$  and the other for  $-\text{C}-\text{H}$  ( $\text{CH}_2$ ,  $\text{CH}_3$ ) group bending vibrations at  $1462.04\text{ cm}^{-1}$  (Carton et al., 2008; Rohman and Che Man, 2011). PLX 407 showed characteristic peaks at  $2885.51\text{ cm}^{-1}$  related to C–H groups,  $1342.46\text{ cm}^{-1}$  corresponding to  $-\text{OH}$  groups, and  $1111.00\text{ cm}^{-1}$  corresponding to C–O groups (Khan et al., 2020). However, the spectrum of the lyophilized optimized formula lacked any of the ZP unique peaks, indicating that ZP was well entrapped inside NLCs.

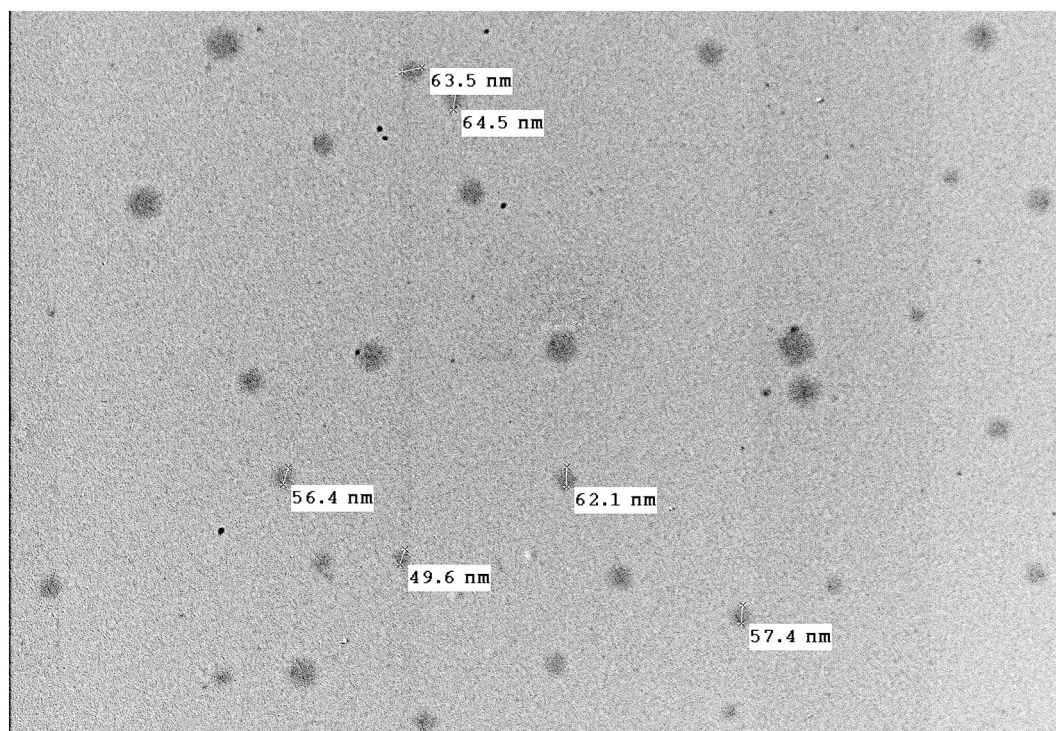


Fig. 6. Transmission electron microscope images of the optimized formula (NLC-OP).

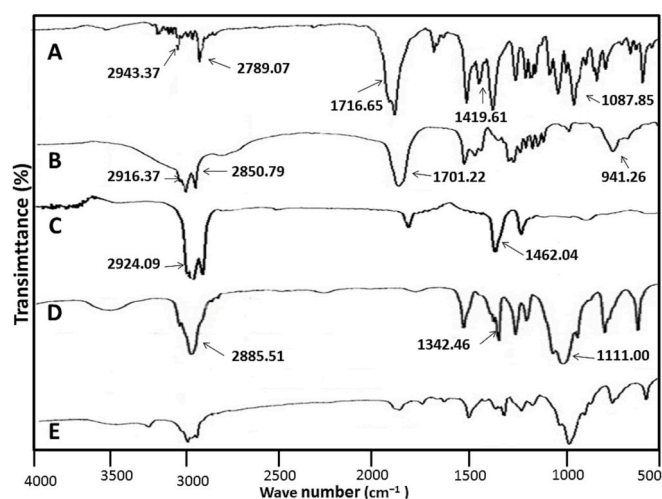


Fig. 7. The FTIR spectra of pure zopiclone (ZP) (A), palmitic acid (PA) (B), cod liver oil (C), poloxamer 407 (PLX 407) (D) and the lyophilized optimized NLCs formula (NLC-OP) (E).

### 3.4.3. Ex vivo cytotoxicity

To foresee any possible toxicity of the optimized ZP-loaded NLCs (NLC-OP) formula to the nasal mucosa, a histopathological assay on excised sheep nasal mucosa was performed. As seen in (Fig. 8), the photomicrographs of the sheep nasal mucosa treated with PBS showed normal histopathological lineaments without any signs of damage to the lining mucosal epithelium with intact underlying structure in both anterior and posterior segments (Fig. 8A&D).

Alternatively, the posterior segment of the sheep nasal mucosa that was tested with isopropyl alcohol showed marked damage and desquamation of the lining mucosal cell layer (Fig. 8E). However, the anterior segment (Fig. 8B), showed no histopathological alteration which could be clarified by the fact that the anterior region of the nasal

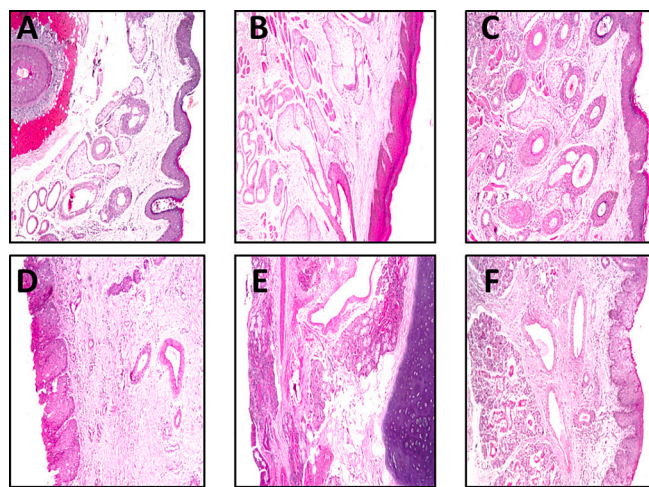


Fig. 8. Histopathological examination of anterior sheep nasal mucosa treated with PBS (pH = 7.4) (A), isopropyl alcohol (B) optimized ZP loaded- NLCs formula (NLC-OP) (C) and posterior sheep nasal mucosa treated with PBS (pH = 7.4) (D), isopropyl alcohol (E), optimized ZP loaded- NLCs formula (NLC-OP) (F).

mucosa is the thicker part of the nasal mucosa with thick keratinized stratified squamous epithelium lining which becomes thinner non-keratinized pseudostratified ciliated columnar respiratory epithelium gradually as we go towards the posterior region (Gao et al., 2020; Gewaily and Abumandour, 2021; Hanafy, 2021; Pathak and Rajput, 2018). This gave some sort of protection to the anterior segment against the damaging effect of isopropyl alcohol.

Eventually, the nasal sheep mucosa exposed to the optimized ZP-loaded NLCs formula (NLC-OP), showed normal histological structure for both anterior and posterior segments (Fig. 8C&F) with unharmed stratified squamous and pseudostratified columnar mucosal epithelia and intact submucosa lining. These returns asserted the safety of the ZP-

loaded NLCs formulation for intranasal administration (Madane and Mahajan, 2016).

### 3.5. Formulation of radioiodinated ZP

Maximum radiolabeling efficiency (RE %) of  $86.34\% \pm 2.59$  was obtained by the addition of  $10 \mu\text{L}$   $^{131}\text{I}\text{NaI}$  to a mixture of  $1 \text{ mg}$  ZP and  $300 \mu\text{g}$  CAT at pH 6 at ambient temperature for 30 min in  $1 \text{ mL}$  total reaction volume. ZP was radioiodinated via direct electrophilic replacement in the existence of oxidizing agent (CAT) (Ibrahim et al., 2015). By studying the aforementioned factors which affected the pathway of the reaction, the obtained RE% depended mainly on the amount of the oxidizing agent which is responsible for the formation of iodonium ion from iodide ion allowing an electrophilic reaction. This critical step was obtained exactly at  $300 \mu\text{g}$  of CAT (Fig. 9A). Variations in the amount of CAT from  $300 \mu\text{g}$  would eventually cause a strong reduction in radiolabeling efficiency, this reduction may occur due to formation of undesirable byproducts at high CAT amounts or due to insufficient oxidation of the radioactive iodine at low CAT amounts (Saha, 2013). The highest RE% was obtained at  $1 \text{ mg}$  of ZP, with lower RE % values at lower drug amount as declared in; (Fig. 9B). This may be due to the absence of sufficient substrates which are required to capture all ( $\text{I}^+$ ) from the solution. On the other hand, there were insignificant changes at amounts higher than  $1 \text{ mg}$  of ZP. The RE% showed a maximum level at pH 6 while at pH lower or  $>6$  the RE% decreased (Fig. 9C) which might be due to the formation of ( $\text{IO}^-$ ) and ( $\text{IO}_3^-$ ) ions that did not participate in the radioiodination process (Sakr, 2014). Also, the reaction time was one of the crucial factors for reaching the

highest RE% value. Reaction times of  $<30 \text{ min}$  were insufficient to complete the reaction (Fig. 9D). Finally the formed  $^{131}\text{I}$ iodo-ZP was stable for  $>24 \text{ h}$ .

#### 3.5.1. Radio formulation of $^{131}\text{I}$ iodo-ZP-NLCs

The  $^{131}\text{I}$ iodo-ZP was formulated with maximum radiolabeling efficiency and then loaded on the optimum NLCs (NLC-OP). The radiolabeling efficiency % of  $^{131}\text{I}$ iodo-ZP-NLCs was reassessed by chromatographic technique to confirm the *in vitro* stability of formulated  $^{131}\text{I}$ iodo-ZP-NLCs. It showed *in vitro* stability with high radiolabeling efficiency of  $>85\%$ .

#### 3.5.2. In vivo biodistribution study

The radioiodinated formulations were administrated to three mice groups (I, II & III) each composed of 18 mice as follows:

- Group I: IN  $^{131}\text{I}$ iodo-ZP-DS
- Group II: IN  $^{131}\text{I}$ iodo-ZP-NLCs
- Group III: IV  $^{131}\text{I}$ iodo-ZP-NLCs

The radioiodinated ZP uptake in blood and brain was determined at predesigned time points up to 4 h revealing ZP concentration (Table 5). Also, (Fig. 10) displays  $^{131}\text{I}$ iodo-ZP concentration in blood (Fig. 10A) and brain (Fig. 10B) after administration of different radioiodinated ZP formulations.

Significantly higher brain concentrations of  $^{131}\text{I}$ iodo-ZP were obtained in Group II ( $6.9 \pm 1.02 \text{ \%ID/g}$  at 5 min post administration) in comparison to the other two groups GP I and GP III ( $2.63 \pm 1.31 \text{ \%ID/g}$

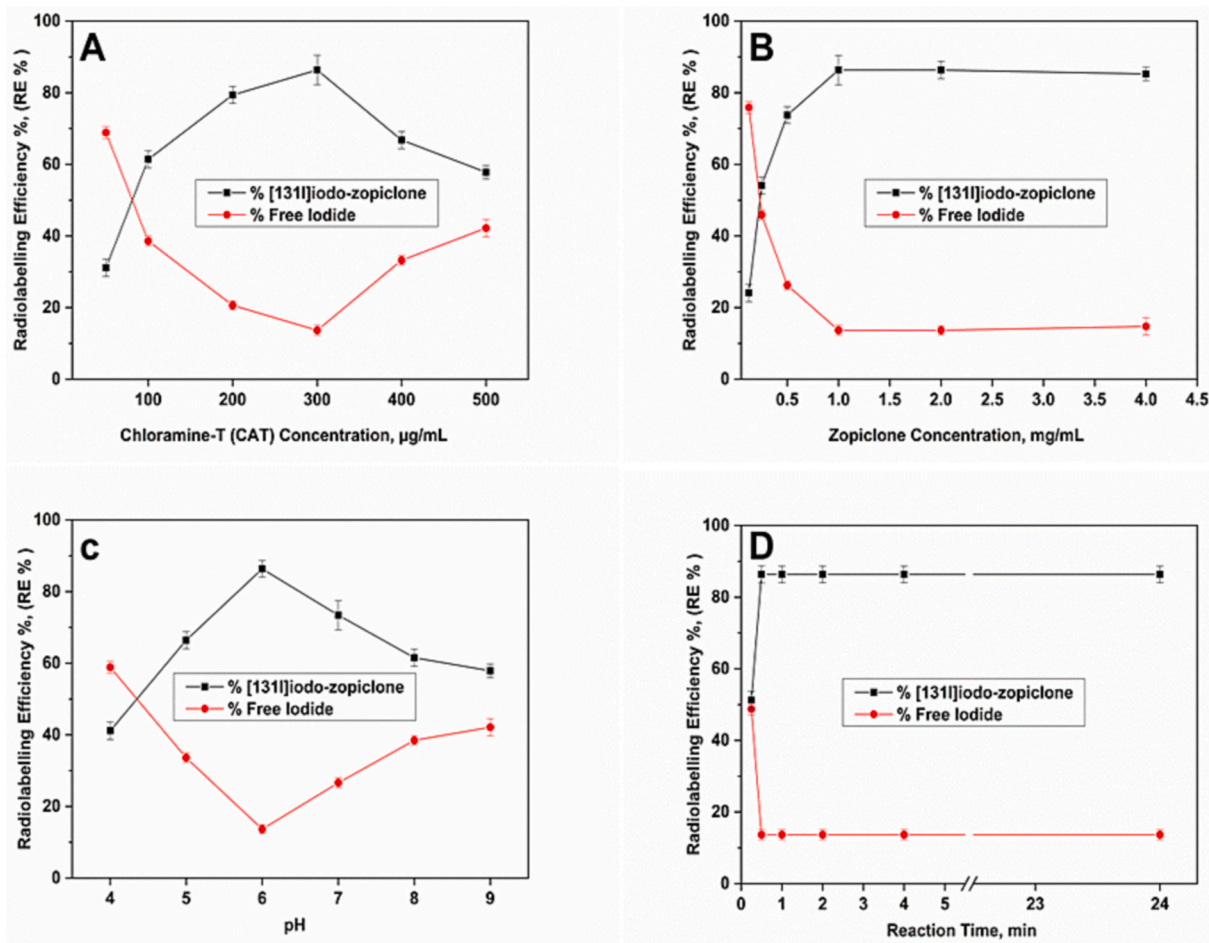
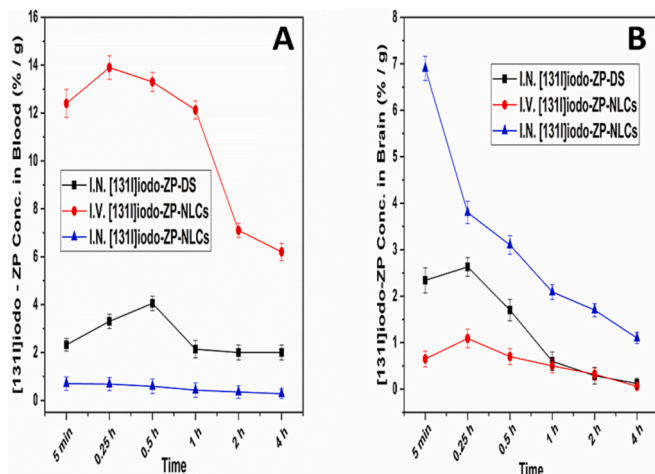


Fig. 9. Variation of the radiolabelling efficiency % (RE%) of  $^{131}\text{I}$ iodo-zopiclone as a function of Chloramine-T (CAT) concentration (A), zopiclone concentration (B), pH (C), reaction time (D).

**Table 5**

Brain, blood ZP conc. and brain/blood ratio of ZP administration as intranasal [<sup>131</sup>I]iodo-ZP-DS, intranasal [<sup>131</sup>I]iodo-ZP-NLCs, and intravenous [<sup>131</sup>I]iodo-ZP-NLCs in male Swiss albino mice (mean ± SD, n = 3).

| Route of administration             | Radioiodinated Formulation | Organ or tissue | Time        |             |             |              |             |             |
|-------------------------------------|----------------------------|-----------------|-------------|-------------|-------------|--------------|-------------|-------------|
|                                     |                            |                 | 5 min       | 0.25 h      | 0.5 h       | 1 h          | 2 h         | 4 h         |
| IN [ <sup>131</sup> I]iodo-ZP-DS    |                            | Brain           | 2.34 ± 1.2  | 2.63 ± 1.31 | 1.7 ± 0.23  | 0.6 ± 0.03   | 0.29 ± 0.02 | 0.12 ± 0.02 |
|                                     |                            | Blood           | 2.32 ± 0.16 | 3.3 ± 0.14  | 4.05 ± 0.3  | 2.14 ± 0.21  | 2 ± 0.15    | 1.90 ± 0.1  |
|                                     |                            | Brain/blood     | 1.01 ± 0.10 | 0.79 ± 0.09 | 0.42 ± 0.07 | 0.28 ± 0.02  | 0.15 ± 0.01 | 0.06 ± 0.00 |
| IN [ <sup>131</sup> I]iodo-ZP- NLCs |                            | Brain           | 6.9 ± 1.02  | 3.8 ± 0.42  | 3.1 ± 0.98  | 2.09 ± 0.81  | 1.7 ± 0.23  | 1.1 ± 0.17  |
|                                     |                            | Blood           | 0.7 ± 0.08  | 0.68 ± 0.09 | 0.59 ± 0.07 | 0.43 ± 0.06  | 0.35 ± 0.02 | 0.28 ± 0.02 |
|                                     |                            | Brain/blood     | 9.9 ± 1.39  | 5.6 ± 0.78  | 5.25 ± 0.48 | 4.9 ± 0.21   | 4.9 ± 0.18  | 3.9 ± 0.12  |
| IV [ <sup>131</sup> I]iodo-ZP-NLCs) |                            | Brain           | 0.65 ± 0.08 | 1.09 ± 0.11 | 0.7 ± 0.08  | 0.5 ± 0.04   | 0.32 ± 0.03 | 0.06 ± 0.00 |
|                                     |                            | Blood           | 12.4 ± 1.61 | 13.9 ± 1.94 | 13.3 ± 1.87 | 12.13 ± 1.48 | 7.1 ± 0.91  | 6.2 ± 0.86  |
|                                     |                            | Brain/blood     | 0.05 ± 0.01 | 0.08 ± 0.01 | 0.05 ± 0.00 | 0.04 ± 0.00  | 0.04 ± 0.00 | 0.01 ± 0.00 |



**Fig. 10.** Blood (A) and Brain (B) ZP concentrations at different time intervals after administration of intranasal [<sup>131</sup>I]iodo-ZP-NLCs, intravenous [<sup>131</sup>I]iodo-ZP-NLCs and [<sup>131</sup>I]iodo-ZP-DS. (mean ± SD, n = 3) in male Swiss albino mice.

and  $1.09 \pm 0.11\%$  ID/g at 0.25 h post-administration, respectively) ( $p < 0.05$ ). Concerning blood samples, higher [<sup>131</sup>I]iodo-ZP concentrations were obtained in GP III in comparison to the other two GPs, this could be owing to the drug being delivered directly to the systemic circulation via the intravenous route.

The brain/blood ratios for various radiolabeled ZP formulations (Table 5) were obtained by dividing the brain [<sup>131</sup>I]iodo-ZP values by the blood values for each animal at the same time point. Significantly greater brain/blood ratios ( $p < 0.05$ ) were noticed in GP II compared to GP I and GP III, demonstrating the improved NLC formula's brain targeting capacity.

The pharmacokinetic characteristics of the three delivered radioiodinated formulations were calculated by computation of  $C_{max}$ ,  $T_{max}$ ,  $AUC_{0-4}$  and  $AUC_{0-\infty}$  for both blood and brain data (Table 6). The significantly higher brain  $C_{max}$ , and  $AUC_{0-\infty}$  values of the IN [<sup>131</sup>I]iodo-ZP- NLCs confirm direct targeting and delivery of the ZP to the brain.

**Table 6**

Pharmacokinetics parameters for ZP administration as intranasal [<sup>131</sup>I]iodo-ZP-DS, intranasal [<sup>131</sup>I]iodo-ZP-NLCs, and intravenous [<sup>131</sup>I]iodo-ZP-NLCs in male Swiss albino mice (mean ± SD, n = 3).

| Formulation/route of administration | Organ or tissue | $C_{max}$ (%ID/g) | $T_{max}$ (h) | $AUC_{0-\infty}$ (h%ID/g) | $AUC_{0-4}$ (h%ID/g) | Relative bioavailability % |
|-------------------------------------|-----------------|-------------------|---------------|---------------------------|----------------------|----------------------------|
|                                     |                 |                   |               |                           |                      |                            |
| IN [ <sup>131</sup> I]iodo-ZP-DS    | Brain           | 2.63 ± 0.01       | 0.25          | 2.70 ± 0.01               | 2.48 ± 0.01          |                            |
|                                     | Blood           | 4.05 ± 0.43       | 0.5           | 59.16 ± 4.05              | 9.00 ± 1.20          |                            |
| IN [ <sup>131</sup> I]iodo-ZP-NLCs  | Brain           | 6.9 ± 0.69        | 0.0833        | 13.17 ± 0.51              | 8.03 ± 0.47          | 487.78 ± 97.66             |
|                                     | Blood           | 0.7 ± 0.20        | 0.0833        | 3.57 ± 0.22               | 1.57 ± 0.22          | 6.04 ± 3.24                |
| IV [ <sup>131</sup> I]iodo-ZP-NLCs  | Brain           | 1.09 ± 0.08       | 0.25          | 1.57 ± 0.33               | 1.48 ± 0.19          |                            |
|                                     | Blood           | 13.9 ± 1.30       | 0.25          | 61.62 ± 17.10             | 35.38 ± 8.48         |                            |

It is clear from the calculated pharmacokinetics parameters that the intranasal administered NLC-OP had a higher ability and greater extent to target the drug to the brain. This was further confirmed mathematically by calculating certain parameters, namely, relative bioavailability, DTE%, DTI, and DTP% (Yasir et al., 2022).

As shown in Table 6, the calculated relative bioavailability was 487.78% and 6.04% for brain and blood, respectively.

DTE%, DTI and DTP% values were 368.69%, 4.57%, 144.58, 1.79 and 99.17%, 44.17% for IN [<sup>131</sup>I]iodo-ZP-DS, IN [<sup>131</sup>I]iodo-ZP-NLCs, respectively (Table 7).

#### 4. Conclusion

In this study, ZP-loaded cod liver oil nano-structured lipid carriers were successfully fabricated utilizing hot emulsification-ultrasonication method for direct nose-to-brain delivery. The optimized formula showed promising results with high EE% confirmed by FTIR spectroscopic analysis and small uniform particle size which facilitate its passage to the brain through nasal mucosa. *Ex vivo* cytotoxicity assay confirmed the safety and tolerability of the nano-structured lipid carriers formulations. Biodistribution and pharmacokinetic study declared that optimized formula was highly and rapidly transported to the brain via the nasal route compared to drug solution or IV administration. In general, presented results indicate that intranasal administration of ZP formulated as nano-structured lipid carriers is a promising technique for enhanced brain delivery.

**Table 7**

DTE%, DTI%, and DTP% of intranasal [<sup>131</sup>I]iodo-ZP-DS and intranasal [<sup>131</sup>I]iodo-ZP-NLCs relative to the intravenous [<sup>131</sup>I]iodo-ZP-NLCs in male Swiss albino mice (mean ± SD, n = 3).

| Formulation/route of administration | DTE%           | DTI            | DTP%         |
|-------------------------------------|----------------|----------------|--------------|
| IN [ <sup>131</sup> I]iodo-ZP-DS    | 4.57 ± 1.01    | 1.79 ± 0.81    | 44.17 ± 7.04 |
| IN [ <sup>131</sup> I]iodo-ZP-NLCs  | 368.69 ± 10.30 | 144.58 ± 10.22 | 99.17 ± 0.04 |

## CRedit author statement

Esraa Taha: Writing - Original Draft, Writing - Review & Editing, Data Curation, Visualization, Conceptualization, Investigation, Validation

Samia A. Nour: Supervision, Visualization, Investigation, Project administration, Validation

Wael Mamdouh: Visualization, Investigation, Supervision, Project administration, Validation

Adli A. Selim: Conceptualization, Methodology, Resources

Mohamed M. Swidan: Conceptualization, Methodology, Resources

Ahmed B. Ibrahim: Conceptualization, Methodology, Resources

Marianne J. Naguib: Writing - Review & Editing, Data Curation, Supervision, Visualization, Conceptualization, Investigation, Validation

## Declaration of Competing Interest

The authors declare that they have no known competing financial interests or personal relationships that could have appeared to influence the work reported in this paper.

## Data availability

All the data are elucidated are presented in the article as mean values and standard deviations

## References

- Abd El-Halim, S.M., Abdelbary, G.A., Amin, M.M., Zakaria, M.Y., Shamsel-Din, H.A., Ibrahim, A.B., 2020. Stabilized oral nanostructured lipid carriers of Adefovir Dipivoxil as a potential liver targeting: Estimation of liver function panel and uptake following intravenous injection of radioiodinated indicator. *DARU. J. Pharm. Sci.* 28, 517–532. <https://doi.org/10.1007/S40199-020-00355-8/FIGURES/8>.
- Abdel Razeq, S.A., Soliman, S.M., Mohamed, A.S., 2018. Validated stability-indicating high-performance liquid chromatography and thin-layer chromatography methods for the determination of zopiclone in pharmaceutical formulation. *J. Planar Chromatogr. Mod. TLC* 31, 297–308. <https://doi.org/10.1556/1006.2018.31.4.5>.
- Abdelhakeem, E., El-Nabarawi, M., Shamma, R., 2021. Lipid-based nano-formulation platform for eplerenone oral delivery as a potential treatment of chronic central serous chorioretinopathy: in-vitro optimization and ex-vivo assessment. *Drug Deliv.* 28, 642–654. <https://doi.org/10.1080/10717544.2021.1902023>.
- Agrahari, Vibhuti, Burnouf, P.-A., Burnouf, T., Agrahari, Vivek, 2019. Nanof ormulation properties, characterization, and behavior in complex biological matrices: challenges and opportunities for brain-targeted drug delivery applications and enhanced translational potential. *Adv. Drug Deliv. Rev.* 148, 146–180. <https://doi.org/10.1016/j.addr.2019.02.008>.
- Agravat, A., 2018. Z'-hypnotics versus benzodiazepines for the treatment of insomnia. *Prog. Neurol. Psychiatry* 22, 26–29. <https://doi.org/10.1002/PNP.502>.
- Agrawal, Y., Patil, K., Mahajan, H., Potdar, M., Joshi, P., Nakhate, K., Sharma, C., Goyal, S.N., Ojha, S., 2022. In vitro and in vivo characterization of Entacapone-loaded nanostructured lipid carriers developed by quality-by-design approach. *Drug Deliv.* 29, 1112–1121. <https://doi.org/10.1080/10717544.2022.2058651>.
- Ahmadi, M., Vahabzadeh, F., Bonakdarpour, B., Mofarragh, E., Mehranian, M., 2005. Application of the central composite design and response surface methodology to the advanced treatment of olive oil processing wastewater using Fenton's peroxidation. *J. Hazard. Mater.* 123, 187–195. <https://doi.org/10.1016/J.JHAZMAT.2005.03.042>.
- Al-Attas, A.S., Nasr, J.J., Shalan, S., Belal, F., 2017. First derivative spectrofluorimetric determination of zopiclone and its degradation product, 2-amino-5-chloropyridine, in pharmaceutical formulations with preliminary tool in biological fluids for clinical evidence of zopiclone intake. *Spectrochim. Acta Part A Mol. Biomol. Spectrosc.* 181, 148–152. <https://doi.org/10.1016/j.saa.2017.03.036>.
- Ali, A.S., Alrashedi, M.G., Ahmed, O.A.A., Ibrahim, I.M., 2022. Pulmonary delivery of hydroxychloroquine nanostructured lipid carrier as a potential treatment of COVID-19. *Polymers (Basel)* 14, 2616. <https://doi.org/10.3390/polym14132616>.
- Apostolou, M., Assi, S., Fatokun, A.A., Khan, I., 2021. The effects of solid and liquid lipids on the physicochemical properties of nanostructured lipid carriers. *J. Pharm. Sci.* 110, 2859–2872. <https://doi.org/10.1016/J.XPHS.2021.04.012>.
- Babazadeh, A., Ghanbarzadeh, B., Hamishehkar, H., 2017. Formulation of food grade nanostructured lipid carrier (NLC) for potential applications in medicinal-functional foods. *J. Drug Deliv. Sci. Technol.* 39, 50–58. <https://doi.org/10.1016/J.JDDST.2017.03.001>.
- Bhattacharya, S., 2021. Central composite design for response surface methodology and its application in pharmacy. *Respos. Surf. Methodol. Eng. Sci.* <https://doi.org/10.5772/INTECHOPEN.95835>.
- Bragg, S., Benich, J.J., Christian, N., Visserman, J., Freedy, J., 2019. Updates in insomnia diagnosis and treatment. *Int. J. Psychiatry Med.* 54, 275–289. <https://doi.org/10.1177/0091217419860716>.
- Brandt, J., Leong, C., 2017. Benzodiazepines and Z-drugs: an updated review of major adverse outcomes reported on in epidemiologic research. *Drugs R D.* <https://doi.org/10.1007/s40268-017-0207-7>.
- Caglar, A., Sahar, T., Cogenli, M.S., Yurtcan, A.B., Aktas, N., Kivrak, H., 2018. A novel central composite design based response surface methodology optimization study for the synthesis of Pd/CNT direct formic acid fuel cell anode catalyst. *Int. J. Hydrog. Energy* 43, 11002–11011. <https://doi.org/10.1016/J.IJHYDENE.2018.04.208>.
- Carton, I., Goicoechea, E., Uriarte, P.S., 2008. Characterization of cod liver oil by spectroscopic techniques. new approaches for the determination of compositional parameters, acyl groups, and cholesterol from 1 H nuclear magnetic resonance and fourier transform infrared spectral data. *J. Agric. Food Chem.* 56, 9072–9079. <https://doi.org/10.1021/jf801834j>.
- Chouinard, G., Lefko-Singh, K., Teboul, E., 1999. Metabolism of anxiolytics and hypnotics: benzodiazepines, buspirone, zopiclone, and zolpidem. *Cell. Mol. Neurobiol.* 19, 533–552. <https://doi.org/10.1023/A:1006943009192>.
- Crowe, T.P., Greenlee, M.H.W., Kanthasamy, A.G., Hsu, W.H., 2018. Mechanism of intranasal drug delivery directly to the brain. *Life Sci.* <https://doi.org/10.1016/j.lfs.2017.12.025>.
- Cunha, S., Costa, C.P., Loureiro, J.A., Alves, J., Peixoto, A.F., Forbes, B., Lobo, J.M.S., Silva, A.C., 2020. Double optimization of rivastigmine-loaded nanostructured lipid carriers (NLC) for nose-to-brain delivery using the quality by design (QbD) approach: formulation variables and instrumental parameters. *Pharm* 12, 599. <https://doi.org/10.3390/PHARMACEUTICS12070599>.
- Danaei, M., Dehghankhold, M., Ataei, S., Hasanzadeh Davarani, F., Javanmard, R., Dokhani, A., Khorasani, S., Mozafari, M., 2018. Impact of particle size and polydispersity index on the clinical applications of lipidic nanocarrier systems. *Pharmaceutics* 10, 57. <https://doi.org/10.3390/pharmaceutics10020057>.
- Dolatnabadi, S., Karimi, M., Nasirizadeh, S., Hatamipour, M., Golmohammadzadeh, S., Jaafari, M.R., 2021. Preparation, characterization and in vivo pharmacokinetic evaluation of curcuminoids-loaded solid lipid nanoparticles (SLNs) and nanostructured lipid carriers (NLCs). *J. Drug Deliv. Sci. Technol.* 62, 102352. <https://doi.org/10.1016/J.JDDST.2021.102352>.
- El-Dahmy, R.M., Elshafeey, A.H., Abd El Gawad, N.A., El-Gazayerly, O.N., Elsayed, I., 2021. Statistical optimization of nanostructured gels for enhancement of vinpocetine transnasal and dermal permeation. *J. Drug Deliv. Sci. Technol.* 66, 102871. <https://doi.org/10.1016/j.jddst.2021.102871>.
- Elmowafy, M., Ibrahim, H.M., Ahmed, M.A., Shalaby, K., Salama, A., Hefesha, H., 2017. Atorvastatin-loaded nanostructured lipid carriers (NLCs): strategy to overcome oral delivery drawbacks. *Drug Deliv.* 24, 932–941. <https://doi.org/10.1080/10717544.2017.1337823>.
- El-Setouhy, D.A., Ibrahim, A.B., Amin, M.M., Khowessah, O.M., Elzanfaly, E.S., 2016. Intranasal haloperidol-loaded miniemulsions for brain targeting: evaluation of locomotor suppression and in-vivo biodistribution. *Eur. J. Pharm. Sci.* 92, 244–254. <https://doi.org/10.1016/J.EJPS.2016.05.002>.
- Fahmy, A.M., El-Setouhy, D.A., Ibrahim, A.B., Habib, B.A., Tayel, S.A., Bayoumi, N.A., 2018. Penetration enhancer-containing spanlastics (PECSs) for transdermal delivery of haloperidol: in vitro characterization, ex vivo permeation and in vivo biodistribution studies. *Drug Deliv.* 25, 12–22. [https://doi.org/10.1080/10717544.2017.1410262/SUPPL\\_FILE/IDRD\\_A\\_1410262\\_SM1831.PDF](https://doi.org/10.1080/10717544.2017.1410262/SUPPL_FILE/IDRD_A_1410262_SM1831.PDF).
- Fathi, H.A., Allam, A., Elsbahy, M., Fetih, G., El-Badry, M., 2018. Nanostructured lipid carriers for improved oral delivery and prolonged antihyperlipidemic effect of simvastatin. *Colloids Surf. B: Biointerfaces* 162, 236–245. <https://doi.org/10.1016/j.colsurfb.2017.11.064>.
- Gadhve, D.G., Kokare, C.R., 2019. Nanostructured lipid carriers engineered for intranasal delivery of teriflunomide in multiple sclerosis: optimization and in vivo studies. *Drug Dev. Ind. Pharm.* 45, 839–851. <https://doi.org/10.1080/03639045.2019.1576724>.
- Gadhve, D., Tupe, S., Tagalpallewar, A., Gorain, B., Choudhury, H., Kokare, C., 2021. Nose-to-brain delivery of amisulpride-loaded lipid-based poloxamer-gellan gum nanoemulgel: in vitro and in vivo pharmacological studies. *Int. J. Pharm.* 607, 121050. <https://doi.org/10.1016/j.ijpharm.2021.121050>.
- Gao, M., Shen, X., Mao, S., 2020. Factors influencing drug deposition in the nasal cavity upon delivery via nasal sprays. *J. Pharm. Investig.* 50, 251–259. <https://doi.org/10.1007/s40005-020-00482-z>.
- Gerber, W., Svitina, H., Steyn, D., Peterson, B., Kotzé, A., Weldon, C., Hamman, J.H., 2022. Comparison of RPMI 2650 cell layers and excised sheep nasal epithelial tissues in terms of nasal drug delivery and immunocytochemistry properties. *J. Pharmacol. Toxicol. Methods* 113, 107131. <https://doi.org/10.1016/j.vascn.2021.107131>.
- Gewaily, M.S., Abumandour, M.M.A., 2021. Gross morphological, histological and scanning electron specifications of the oropharyngeal cavity of the hooded crow (*Corvus cornix pallescens*). *Anat. Histol. Embryol.* 50, 72–83. <https://doi.org/10.1111/ahel.12602>.
- Ghelich, R., Jahannama, M.R., Abdizadeh, H., Torknik, F.S., Vaezi, M.R., 2019. Central composite design (CCD)-Response surface methodology (RSM) of effective electrospinning parameters on PVP-B-Hf hybrid nanofibrous composites for synthesis of HfB<sub>2</sub>-based composite nanofibers. *Compos. Part B Eng.* 166, 527–541. <https://doi.org/10.1016/J.COMPOSITESB.2019.01.094>.
- Goa, K.L., Heel, R.C., 1986. Zopiclone. *Drugs* 32, 48–65. <https://doi.org/10.2165/00003495-198632010-00003>.
- Gupta, N., Gupta, S.M., Sharma, S.K., 2021. Synthesis, characterization and dispersion stability of water-based Cu-CNT hybrid nanofluid without surfactant. *Microfluid. Nanofluid.* 25, 1–14. <https://doi.org/10.1007/S10404-021-02421-2/TABLES/9>.

- Haider, M., Abidin, S.M., Kamal, L., Orive, G., 2020. Nanostructured lipid carriers for delivery of chemotherapeutics: a review. *Pharm* 12, 288. <https://doi.org/10.3390/PHARMACEUTICS12030288>.
- Hanafy, B.G., 2021. Structural adaptation of the nasal conchae of Eurasian common moorhen (*Gallinula chloropus chloropus*, Linnaeus, 1758)—Histomorphological study. *Microsc. Res. Tech.* 84, 2195–2202. <https://doi.org/10.1002/jemt.23778>.
- Hassan, D.H., Shohdy, J.N., El-Setouhy, D.A., El-Nabarawi, M., Naguib, M.J., 2022. Compritol-based nanostructured lipid carriers (NLCs) for augmentation of zolmitriptan bioavailability via the transdermal route: in vitro optimization, ex vivo permeation, in vivo pharmacokinetic study. *Pharmaceutics* 14, 1484. <https://doi.org/10.3390/pharmaceutics14071484>.
- Hesse, L.M., von Moltke, L.L., Greenblatt, D.J., 2003. Clinically important drug interactions with zopiclone, zolpidem and zaleplon. *CNS Drugs* 17, 513–532. <https://doi.org/10.2165/00023210-200317070-00004>.
- Houacine, C., Adams, D., Singh, K.K., 2020. Impact of liquid lipid on development and stability of trimyristin nanostructured lipid carriers for oral delivery of resveratrol. *J. Mol. Liq.* 316, 113734. <https://doi.org/10.1016/j.molliq.2020.113734>.
- Ibrahim, A.B., Sakr, T.M., Khoweisa, O.M.A., Motaleb, M.A., Abd El-Bary, A., El-Kolaly, M.T., 2015. Radioiodinated anastrozole and epirubicin as potential targeting radiopharmaceuticals for solid tumor imaging. *J. Radioanal. Nucl. Chem.* 303, 967–975. <https://doi.org/10.1007/S10967-014-3560-9/FIGURES/13>.
- Ibrahim, A.B., Alaraby Salem, M., Fasih, T.W., Brown, A., Sakr, T.M., 2018. Radioiodinated doxorubicin as a new tumor imaging model: preparation, biological evaluation, docking and molecular dynamics. *J. Radioanal. Nucl. Chem.* 317, 1243–1252. <https://doi.org/10.1007/S10967-018-6013-Z/FIGURES/9>.
- Javaheri, S., Redline, S., 2017. Insomnia and risk of cardiovascular disease. *Chest*. <https://doi.org/10.1016/j.chest.2017.01.026>.
- Joseph Naguib, M., Moustafa Kamel, A., Thabet Negmeldin, A., Elshafeey, A.H., Elsayed, I., 2020. Molecular docking and statistical optimization of taurocholate-stabilized galactose anchored bilosomes for the enhancement of sofosbuvir absorption and hepatic relative targeting efficiency. *Drug Deliv.* 27, 996–1009. <https://doi.org/10.1080/10717544.2020.1787557>.
- Kataria, D., Zafar, A., Ali, J., Khatoun, K., Khan, S., Imam, S.S., Yasir, M., Ali, A., 2022. Formulation of lipid-based nanocarriers of lacidipine for improvement of oral delivery: Box-Behnken design optimization, in vitro, ex vivo, and preclinical assessment. *Assay Drug Dev. Technol.* 20, 5–21. <https://doi.org/10.1089/ADT.2021.084/ASSET/IMAGES/LARGE/ADT.2021.084.FIGURES.JPEG>.
- Katopodi, A., Detsi, A., 2021. Solid lipid nanoparticles and nanostructured lipid carriers of natural products as promising systems for their bioactivity enhancement: the case of essential oils and flavonoids. *Colloids Surf. A Physicochem. Eng. Asp.* 630, 127529. <https://doi.org/10.1016/J.COLSURFA.2021.127529>.
- Keller, L.-A., Merkel, O., Popp, A., 2022. Intranasal drug delivery: opportunities and toxicological challenges during drug development. *Drug Deliv. Transl. Res.* 12, 735–757. <https://doi.org/10.1007/s13346-020-00891-5>.
- Khan, K.A., CT, R., 1972. Effect of Compaction Pressure on the Dissolution Efficiency of some Direct Compression Systems.
- Khan, K.U., Akhtar, N., Minhas, M.U., 2020. Poloxamer-407-Co-poly (2-acrylamido-2-methylpropane sulfonic acid) cross-linked nanogels for solubility enhancement of olanzapine: synthesis, characterization, and toxicity evaluation. *AAPS PharmSciTech* 21, 1–15. <https://doi.org/10.1208/S12249-020-01694-0/TABLES/5>.
- Khan, A.S., Din, F., Ali, Z., Bibi, M., Zahid, F., Zeb, A., Mujeeb-ur-Rehman, Khan, G.M., 2021. Development, in vitro and in vivo evaluation of miltfosfene loaded nanostructured lipid carriers for the treatment of Cutaneous Leishmaniasis. *Int. J. Pharm.* 593, 120109. <https://doi.org/10.1016/j.ijpharm.2020.120109>.
- Koch-Weser, J., Greenblatt, D.J., Shader, R.I., Abernethy, D.R., 1983. Current status of benzodiazepines. *N. Engl. J. Med.* 309, 410–416. <https://doi.org/10.1056/NEJM198308183090705>.
- Kovačević, A.B., Müller, R.H., Keck, C.M., 2020. Formulation development of lipid nanoparticles: improved lipid screening and development of tacrolimus loaded nanostructured lipid carriers (NLC). *Int. J. Pharm.* 576, 118918. <https://doi.org/10.1016/j.ijpharm.2019.118918>.
- Kraisit, P., Sarisuta, N., 2018. Development of triamcinolone acetone-loaded nanostructured lipid carriers (NLCs) for buccal drug delivery using the Box-Behnken design. *Molecules* 23, 982. <https://doi.org/10.3390/molecules23040982>.
- Kumbhar, S.A., Kokare, C.R., Shrivastava, B., Gorain, B., Choudhury, H., 2021. Antipsychotic potential and safety profile of TPGS-based mucoadhesive aripiprazole nanoemulsion: development and optimization for nose-to-brain delivery. *J. Pharm. Sci.* 110, 1761–1778. <https://doi.org/10.1016/j.xphs.2021.01.021>.
- Lombardo, R., Musumeci, T., Carbone, C., Pignatello, R., 2021. Nanotechnologies for intranasal drug delivery: an update of literature. *Pharm. Dev. Technol.* 26, 824–845. <https://doi.org/10.1080/10837450.2021.1950186>.
- Louzada, L.L., Machado, F.V., Nóbrega, O.T., Camargos, E.F., 2021a. Zopiclone to treat insomnia in older adults: a systematic review. *Eur. Neuropsychopharmacol.* 50, 75–92. <https://doi.org/10.1016/j.euroneuro.2021.04.013>.
- Louzada, L.L., Machado, F.V., Quintas, J.L., Ribeiro, G.A., Silva, M.V., Mendonça-Silva, D.L., Gonçalves, B.S.B., Nóbrega, O.T., Camargos, E.F., 2021b. The efficacy and safety of zolpidem and zopiclone to treat insomnia in Alzheimer's disease: a randomized, triple-blind, placebo-controlled trial. *Neuropsychopharmacology* 47(4), 570–579. <https://doi.org/10.1038/s41386-021-01191-3>.
- Madane, R.G., Mahajan, H.S., 2016. Curcumin-loaded nanostructured lipid carriers (NLCs) for nasal administration: design, characterization, and in vivo study. *Drug Deliv.* 23, 1326–1334. <https://doi.org/10.3109/10717544.2014.975382>.
- Mahajan, H., Patil, N., 2021. Nanoemulsion containing a synergistic combination of curcumin and quercetin for nose-to-brain delivery: in vitro and in vivo studies. *Asian Pac. J. Trop. Biomed.* 11, 510. <https://doi.org/10.4103/2221-1691.328058>.
- Mahmood, A., Rapalli, V.K., Gorantla, S., Waghule, T., Singhvi, G., 2021. Dermatokinetic assessment of luliconazole-loaded nanostructured lipid carriers (NLCs) for topical delivery: QbD-driven design, optimization, and in vitro and ex vivo evaluations. *Drug Deliv. Transl. Res.* 1–18. <https://doi.org/10.1007/S13346-021-00986-7/TABLES/6>.
- Makoni, P.A., Kasongo, K.W., Walker, R.B., 2019. Short term stability testing of efavirenz-loaded solid lipid nanoparticle (SLN) and nanostructured lipid carrier (NLC) dispersions. *Pharm* 11, 397. <https://doi.org/10.3390/PHARMACEUTICS11080397>.
- Mani, A., Ebrahimi, E., 2022. Equally weighted multivariate optimization of feeding rate for sub-yearling great sturgeon (*Huso huso*) using desirability function model. *J. World Aquacult. Soc.* 53, 693–702. <https://doi.org/10.1111/jwas.12857>.
- Mattos, M.K., Chang, A., Pitcher, K., Whitt, C., Ritterband, L.M., Quigg, M.S., 2021. A review of insomnia treatments for patients with mild cognitive impairment. *Aging Dis.* 12, 1036. <https://doi.org/10.14336/AD.2021.0423>.
- Medina-Montano, C., Rivero Berti, I., Gambaro, R., Limeres, M., Svensson, M., Padula, G., Chain, C., Cisneros, J., Castro, G., Grabbe, S., Bros, M., Gehring, S., Islan, G., Cacicedo, M., 2022. Nanostructured lipid carriers loaded with dexamethasone prevent inflammatory responses in primary non-parenchymal liver cells. *Pharmaceutics* 14, 1611. <https://doi.org/10.3390/pharmaceutics14081611>.
- de Mendonça, F.M.R., de Mendonça, G.P.R.R., Souza, L.C., Galvao, L.P., Paiva, H.S., Perico, C.A.M., Torales, J., Ventriglio, A., Castaldelli-Maia, J.M., Martins Silva, A.S., 2021. Benzodiazepines and sleep architecture: a systematic review. *CNS Neurol. Disord. Drug Targets* 20. <https://doi.org/10.2174/1871527320666210618103344>.
- Ming, X., Lian, H., Zhu, W., 2007. Spectral data analyses and structure elucidation of sedative-hypnotic zopiclone. *Instrum. Sci. Technol.* 35, 349–360. <https://doi.org/10.1080/10739140701255656>.
- Moreno-Bautista, G., Tam, K.C., 2011. Evaluation of dialysis membrane process for quantifying the in vitro drug-release from colloidal drug carriers. *Colloids Surf. A Physicochem. Eng. Asp.* 389, 299–303. <https://doi.org/10.1016/j.colsurfa.2011.07.032>.
- Motaleb, M.A., El-Kolaly, M.T., Ibrahim, A.B., Abd El-Bary, A., 2011. Study on the preparation and biological evaluation of 99mTc-gatifloxacin and 99mTc-cefepime complexes. *J. Radioanal. Nucl. Chem.* 289, 57–65. <https://doi.org/10.1007/S10967-011-1058-2>.
- Moura, R.P., Martins, C., Pinto, S., Sousa, F., Sarmento, B., 2019. Blood-brain barrier receptors and transporters: an insight on their function and how to exploit them through nanotechnology. *Expert Opin. Drug Deliv.* 16, 271–285. <https://doi.org/10.1080/17425247.2019.1583205>.
- Mura, P., Maestrelli, F., D'Ambrosio, M., Luceri, C., Cirri, M., 2021. Evaluation and comparison of solid lipid nanoparticles (SLNs) and nanostructured lipid carriers (NLCs) as vectors to develop hydrochlorothiazide effective and safe pediatric oral liquid formulations. *Pharm* 13, 437. <https://doi.org/10.3390/PHARMACEUTICS13040437>.
- Nagaraja, S., Basavarajappa, G.M., Karnati, R.K., Bakir, E.M., Pund, S., 2021. Ion-triggered in situ gelling nanoemulgel as a platform for nose-to-brain delivery of small lipophilic molecules. *Pharmaceutics* 13, 1216. <https://doi.org/10.3390/pharmaceutics13081216>.
- Naguib, M.J., Salah, S., Abdel Halim, S.A., Badr-Eldin, S.M., 2020. Investigating the potential of utilizing glycosomes as a novel vesicular platform for enhancing intranasal delivery of lacidipine. *Int. J. Pharm.* 582, 119302. <https://doi.org/10.1016/j.ijpharm.2020.119302>.
- Naguib, M.J., Hassan, Y.R., Abd-ElSalam, W.H., 2021. 3D printed ocusert laden with ultra-fluidic glycosomes of ganciclovir for the management of ocular cytomegalovirus retinitis. *Int. J. Pharm.* 607, 121010. <https://doi.org/10.1016/j.ijpharm.2021.121010>.
- Najib, J.S., 2010. Efficacy and safety of zopiclone and eszopiclone in the treatment of primary and comorbid insomnia. In: *GABA and Sleep*. Springer Basel, Basel, pp. 413–451. [https://doi.org/10.1007/978-3-0346-0226-6\\_18](https://doi.org/10.1007/978-3-0346-0226-6_18).
- Noble, S., Langtry, H.D., Lamb, H.M., 1998. Zopiclone. *Drugs* 55, 277–302. <https://doi.org/10.2165/00003495-199855020-00015>.
- Nour, S.A., Abdelmalak, N.S., Naguib, M.J., Rashed, H.M., Ibrahim, A.B., 2016. Intranasal brain-targeted clonazepam polymeric micelles for immediate control of status epilepticus: in vitro optimization, ex vivo determination of cytotoxicity, in vivo biodistribution and pharmacodynamics studies. *Drug Deliv.* 23, 3681–3695. <https://doi.org/10.1080/10717544.2016.1223216>.
- Pathak, V., Rajput, R., 2018. Histological and histochemical studies on the nasal cavity of gaddi sheep. *Indian J. Small Ruminants* 24, 281. <https://doi.org/10.5958/0973-9718.2018.00050.8>.
- Pradhan, M., Alexander, A., Singh, M.R., Singh, D., Saraf, Swarnlata, Saraf, Shailendra, Yadav, K., Ajazuddin, 2021. Statistically optimized calcipotriol fused nanostructured lipid carriers for effective topical treatment of psoriasis. *J. Drug Deliv. Sci. Technol.* 61, 102168. <https://doi.org/10.1016/j.jddst.2020.102168>.
- Rohman, A., Che Man, Y.B., 2011. Application of Fourier transform infrared (FT-IR) spectroscopy combined with chemometrics for authentication of cod-liver oil. *Vib. Spectrosc.* 55, 141–145. <https://doi.org/10.1016/j.vibspec.2010.10.001>.
- Saeedi, M., Eslamifard, M., Khezri, K., Dizaj, S.M., 2019. Applications of nanotechnology in drug delivery to the central nervous system. *Biomed. Pharmacother.* 111, 666–675. <https://doi.org/10.1016/j.biopha.2018.12.133>.
- Saha, G.B., 2013. Physics and radiobiology of nuclear medicine. *Phys. Radiobiol. Nucl. Med.* 1–356. <https://doi.org/10.1007/978-1-4614-4012-3>.
- Sahu, T., Ratre, Y.K., Chauhan, S., Bhaskar, L.V.K.S., Nair, M.P., Verma, H.K., 2021. Nanotechnology based drug delivery system: current strategies and emerging therapeutic potential for medical science. *J. Drug Deliv. Sci. Technol.* 63, 102487. <https://doi.org/10.1016/j.jddst.2021.102487>.

- Sakr, T.M., 2014. Synthesis and preliminary affinity testing of 123I/125I-N-(3-iodophenyl)-2-methylpyrimidine-4,6-diamine as a novel potential lung scintigraphic agent. *Radiochem* 562 (56), 200–206. <https://doi.org/10.1134/S1066362214020131>.
- Sakr, T.M., Ibrahim, A.B., Fasih, T.W., Rashed, H.M., 2017. Preparation and biological profile of <sup>99m</sup>Tc-lidocaine as a cardioselective imaging agent using <sup>99m</sup>Tc eluted from <sup>99m</sup>Mo/<sup>99m</sup>Tc generator based on Al–Mo gel. *J. Radioanal. Nucl. Chem.* 314, 2091–2098. <https://doi.org/10.1007/S10967-017-5560-Z/FIGURES/9>.
- Samadi, N., Aberoomand Azar, P., Waqif Husain, S., Maibach, H.I., Nafisi, S., 2020. Experimental design in formulation optimization of vitamin K1 oxide-loaded nanoliposomes for skin delivery. *Int. J. Pharm.* 579, 119136 <https://doi.org/10.1016/j.ljpharm.2020.119136>.
- Sanad, R.A., Abdelmalak, N.S., Elbayoomy, T.S., Badawi, A.A., 2010. Formulation of a novel oxybenzone-loaded nanostructured lipid carriers (NLCs). *AAPS PharmSciTech* 11, 1684–1694. <https://doi.org/10.1208/S12249-010-9553-2/FIGURES/8>.
- Sayed, S., Elsharkawy, F.M., Amin, M.M., Shamsel-Din, H.A., Ibrahim, A.B., 2021. Brain targeting efficiency of intranasal clozapine-loaded mixed micelles following radio labeling with Technetium-99m, 28, pp. 1524–1538. <https://doi.org/10.1080/10717544.2021.1951895>.
- Serralheiro, A., Alves, G., Fortuna, A., Falcão, A., 2014. Intranasal administration of carbamazepine to mice: a direct delivery pathway for brain targeting. *Eur. J. Pharm. Sci.* 60, 32–39. <https://doi.org/10.1016/j.ejps.2014.04.019>.
- Shaghlil, L., Alshishani, A., Sa'aleek, A.A., Abdelkader, H., Al-ebini, Y., 2022. Formulation and evaluation of nasal insert for nose-to-brain drug delivery of rivastigmine tartrate. *J. Drug Deliv. Sci. Technol.* 76, 103736 <https://doi.org/10.1016/j.jddst.2022.103736>.
- Shamsel-Din, H.A., Ibrahim, A.B., 2017. A novel radiolabeled indole derivative as solid tumor imaging agent: in silico and preclinical pharmacological study. *J. Radioanal. Nucl. Chem.* 314, 2263–2269. <https://doi.org/10.1007/S10967-017-5551-0/FIGURES/8>.
- Sharma, G., Sharma, A.R., Lee, S.-S., Bhattacharya, M., Nam, J.-S., Chakraborty, C., 2019. Advances in nanocarriers enabled brain targeted drug delivery across blood brain barrier. *Int. J. Pharm.* 559, 360–372. <https://doi.org/10.1016/j.ijpharm.2019.01.056>.
- Shinde, G., Sonchhatra, A., Shelke, S., Pathan, I., 2022. Design, optimization and in-vivo characterization of mupirocin loaded nanostructured lipid carrier based gel for effective treatment of impetigo. *J. Drug Deliv. Sci. Technol.* 67, 102872 <https://doi.org/10.1016/j.jddst.2021.102872>.
- Shirazi, A.S., Varshochian, R., Rezaei, M., Ardakani, Y.H., Dinarvand, R., 2021. SN38 loaded nanostructured lipid carriers (NLCs); preparation and in vitro evaluations against glioblastoma. *J. Mater. Sci. Mater. Med.* 32, 1–12. <https://doi.org/10.1007/S10856-021-06538-2/TABLES/4>.
- da Silva, M.G., de Godoi, K.R.R., Gigante, M.L., Cardoso, L.P., Ribeiro, A.P.B., 2022. Nanostructured lipid carriers for delivery of free phytosterols: effect of lipid composition and chemical interesterification on physical stability. *Colloids Surf. A Physicochem. Eng. Asp.* 640, 128425 <https://doi.org/10.1016/j.colsurfa.2022.128425>.
- Singh, A.P., Sharma, S.K., Gaur, P.K., Gupta, D.K., 2021. Fabrication of mupirocin-loaded nanostructured lipid carrier and its in vitro characterization. *Assay Drug Dev. Technol.* 19, 216–225. <https://doi.org/10.1089/ADT.2020.1070/ASSET/IMAGES/LARGE/ADT.2020.1070.FIGURE6.JPEG>.
- de Souza, I.D.L., Saez, V., de Campos, V.E.B., Mansur, C.R.E., 2019. Size and vitamin E release of nanostructured lipid carriers with different liquid lipids, surfactants and preparation methods. *Macromol. Symp.* 383, 1800011. <https://doi.org/10.1002/MASY.201800011>.
- Tan, M.S.A., Parekh, H.S., Pandey, P., Siskind, D.J., Falconer, J.R., 2020. Nose-to-brain delivery of antipsychotics using nanotechnology: a review. *Expert Opin. Drug Deliv.* 17, 839–853. <https://doi.org/10.1080/17425247.2020.1762563>.
- Teleanu, D., Chircov, C., Grumezescu, A., Volceanov, A., Teleanu, R., 2018. Blood-brain delivery methods using nanotechnology. *Pharmaceutics* 10, 269. <https://doi.org/10.3390/pharmaceutics10040269>.
- Terblanche, R.J., Liebenberg, W., De Villiers, M.M., Lötter, A.P., 2000. Characterization of zopiclone crystal forms found among generic raw materials. *Drug Dev. Ind. Pharm.* 26, 531–537. <https://doi.org/10.1081/DDC-100101264>.
- Tetyczka, C., Griesbacher, M., Absenger-Novak, M., Fröhlich, E., Roblegg, E., 2017. Development of nanostructured lipid carriers for intraoral delivery of Domperidone. *Int. J. Pharm.* 526, 188–198. <https://doi.org/10.1016/j.ijpharm.2017.04.076>.
- Tetyczka, C., Hodzic, A., Kriechbaum, M., Juraić, K., Spirk, C., Hartl, S., Pritz, E., Leitinger, G., Roblegg, E., 2019. Comprehensive characterization of nanostructured lipid carriers using laboratory and synchrotron X-ray scattering and diffraction. *Eur. J. Pharm. Biopharm.* 139, 153–160. <https://doi.org/10.1016/j.ejpb.2019.03.017>.
- Thapa, R.K., Cazzador, F., Grønlien, K.G., Tønnesen, H.H., 2020. Effect of curcumin and cosolvents on the micellization of Pluronic F127 in aqueous solution. *Colloids Surf. B: Biointerfaces* 195, 111250. <https://doi.org/10.1016/J.COLSURFB.2020.111250>.
- Tsai, M.J., Wu, P.C., Huang, Y. Bin, Chang, J.S., Lin, C.L., Tsai, Y.H., Fang, J.Y., 2012. Baicalein loaded in tocot nanostructured lipid carriers (tocot NLCs) for enhanced stability and brain targeting. *Int. J. Pharm.* 423, 461–470. <https://doi.org/10.1016/j.ijpharm.2011.12.009>.
- Van Someren, E.J.W., 2021. Brain mechanisms of insomnia: new perspectives on causes and consequences. *Physiol. Rev.* 101, 995–1046. <https://doi.org/10.1152/PHYSREV.00046.2019/ASSET/IMAGES/MEDIUM/PRV-00046-2019R01.PNG>.
- Verekar, R.R., Gurav, S.S., Bolmal, U., 2020. Thermosensitive mucoadhesive in situ gel for intranasal delivery of Almotriptan malate: formulation, characterization, and evaluation. *J. Drug Deliv. Sci. Technol.* 58, 101778 <https://doi.org/10.1016/j.jddst.2020.101778>.
- Weitzer, J., Papantoniou, K., Lázaro-Sebastià, C., Seidel, S., Klösch, G., Schernhammer, E., 2021. The contribution of dispositional optimism to understanding insomnia symptomatology: Findings from a cross-sectional population study in Austria. *J. Sleep Res.* 30, e13132 <https://doi.org/10.1111/JSR.13132>.
- Wu, B., Zhao, Y., Liu, Q., Zhou, C., Zhang, X., Lei, J., 2019. Form-stable phase change materials based on castor oil and palmitic acid for renewable thermal energy storage. *J. Therm. Anal. Calorim.* 137, 1225–1232. <https://doi.org/10.1007/s10973-019-08041-x>.
- Wu, K.W., Sweeney, C., Dudhipala, N., Lakhani, P., Chaurasiya, N.D., Tekwani, B.L., Majumdar, S., 2021. Primaquine loaded solid lipid nanoparticles (SLN), nanostructured lipid carriers (NLC), and nanoemulsion (NE): effect of lipid matrix and surfactant on drug entrapment, in vitro release, and ex vivo hemolysis. *AAPS PharmSciTech* 22, 1–12. <https://doi.org/10.1208/S12249-021-02108-5/FIGURES/7>.
- Yasir, M., Zafar, A., Noorulla, K.M., Tura, A.J., Sara, U.V.S., Panjwani, D., Khalid, M., Haji, M.J., Gobena, W.G., Gebissa, T., Dalecha, D.D., 2022. Nose to brain delivery of donepezil through surface modified NLCs: Formulation development, optimization, and brain targeting study. *J. Drug Deliv. Sci. Technol.* 75, 103631 <https://doi.org/10.1016/j.jddst.2022.103631>.
- Zaami, S., Graziano, S., Tittarelli, R., Beck, R., Marinelli, E., 2021. BDZs, designer BDZs and Z-drugs: pharmacology and misuse insights. *Curr. Pharm. Des.* 27 <https://doi.org/10.2174/1381612827666210917145636>.
- Zafar, A., Alruwaili, N.K., Imam, S.S., Alsaidan, O.A., Alharbi, K.S., Yasir, M., Elmowafy, M., Mohammed, E.F., Al-Oanzi, Z.H., 2021. Formulation of chitosan-coated piperine NLCs: optimization, in vitro characterization, and in vivo preclinical assessment. *AAPS PharmSciTech* 22, 1–16. <https://doi.org/10.1208/S12249-021-02098-4/TABLES/6>.
- Zafar, A., Imam, S.S., Yasir, M., Alruwaili, N.K., Alsaidan, O.A., Warsi, M.H., Ullah, S.N. M.N., Alshehri, S., Ghoneim, M.M., 2022. Preparation of NLCs-based topical erythromycin gel: in vitro characterization and antibacterial assessment. *Gels* 8, 116. <https://doi.org/10.3390/GELS8020116>.
- Zhang, Z., Guan, J., Jiang, Z., Yang, Y., Liu, J., Hua, W., Mao, Y., Li, C., Lu, W., Qian, J., Zhan, C., 2019. Brain-targeted drug delivery by manipulating protein corona functions. *Nat. Commun.* 10, 3561. <https://doi.org/10.1038/s41467-019-11593-z>.
- Zhou, Y., Li, L., Liu, Z., Wang, Q., Zhou, Q., Zhou, W., 2020. Development and evaluation of zopiclone compression coated tablet for time-controlled pulse release: Mechanism and in vivo study. *J. Drug Deliv. Sci. Technol.* 57, 101714 <https://doi.org/10.1016/j.jddst.2020.101714>.
- Zhu, Q.-Y., Guissi, F., Yang, R.-Y., Wang, Q., Wang, K., Chen, D., Han, Z.-H., Ma, Y., Zhang, M., Gu, Y.-Q., 2015. Preparation of Deep Sea fish Oil-based Nanostructured Lipid Carriers with Enhanced Cellular Uptake. *J. Nanosci. Nanotechnol.* 15, 9539–9547. <https://doi.org/10.1166/jnn.2015.10880>.